Changes in the surface and atmospheric water budget due to projected Amazon deforestation: Lessons from a fully coupled model simulation

Sly Wongchuig, Jhan Carlo Espinoza, Thomas Condom, Clementine Junquas, Juan Pablo Sierra, Lluís Fita, Anna Sörensson, Jan Polcher

Journal of Hydrology 625 (2023) 130082

Contents lists available at ScienceDirect

Journal of Hydrology

journal homepage: www.elsevier.com/locate/jhydrol

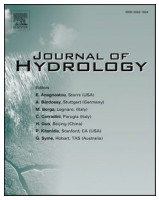

Research papers

Changes in the surface and atmospheric water budget due to projected Amazon deforestation: Lessons from a fully coupled model simulation

Sly Wongchuig [a,*], Jhan Carlo Espinoza [a], Thomas Condom [a], Clementine Junquas [a], Juan Pablo Sierra [a], Lluís Fita [b,c,d], Anna Sörensson [b,c,d], Jan Polcher [e]

[a] Univ. Grenoble Alpes, IRD, CNRS, Grenoble INP, Institut des Géosciences de l'Environnement (IGE, UMR 5001), Grenoble, France
[b] Facultad de Ciencias Exactas y Naturales, Universidad de Buenos Aires, Buenos Aires, Argentina
[c] Centro de Investigaciones del Mar y la Atmósfera (CIMA), CONICET – Universidad de Buenos Aires, Buenos Aires, Argentina
[d] Instituto Franco-Argentino para el Estudio del Clima y sus Impactos (IRL 3351 IFAECI), CNRS – IRD – CONICET – UBA, Buenos Aires, Argentina
[e] Laboratoire de Météorologie Dynamique (LMD), IPSL, CNRS, École Polytechnique, Palaisseau, France

ARTICLE INFO

This manuscript was handled by Marco Borga, Editor-in-Chief, with the assistance of Yadu Pokhrel, Associate Editor

Keywords:
Coupled land–atmosphere modeling
Future Amazon deforestation
Changes in water budget

ABSTRACT

The Amazon forest has a complex interaction with climate at different spatial and temporal scales. This means that alterations in land use could modify the regional water cycle, including the surface and atmospheric water budget. However, little is known about how these changes occur seasonally and in a spatially distributed manner in the most vulnerable regions, such as the southern Amazon. In this study, the local to regional effects of future Amazon deforestation on the surface and atmospheric water budget components are investigated by twin numerical experiments using the Regional Earth System Model of the 'Institute Pierre Simone Laplace' (RegIPSL) for 19 yr (2001–2019). The results show that significant changes in precipitation and actual evapotranspiration in the southern Amazon (south of 5°S) are associated with surrounding areas with a deforested ratio higher than 40%. During the onset of the wet season (September-November) the largest changes in convective processes are manifested by opposite atmospheric dynamic in adjacent regions (dipole), associated with. This dynamic is associated with wind orientation and the different sizes of the straight corridors of continuous deforestation (pathways). The dipole manifests itself as a suppression of convection in the upwind sector, while convection increases in the downwind sector of the deforestation pathway. For medium-sized deforestation pathways (~350 km) convection changes are related to dynamic processes (decrease in surface roughness). In large-sized pathways (~500 km) the mechanisms causing convective changes are combined, dynamic and thermal (increase in surface temperature). In deforested regions there is an average increase of terrestrial water storage dynamics and runoff ~10 times higher than in non-deforested regions. Furthermore, the atmosphere becomes ~8 times drier in deforested regions than in non-deforested regions. Our findings indicate a new perspective regarding a comprehensive modeling approach to understand potential changes in the surface and atmospheric water cycle in different regions of Amazonia and in different seasons due to future deforestation and thus provide new insights into their spatial and temporal variability at sub-regional scales.

1. Introduction

The Amazon basin is the largest rainforest in the world, where vegetation and climate are strongly interdependent and exchange energy, moisture and momentum in a dynamic equilibrium (Salati and Nobre, 1991; Zemp et al., 2017; Zeng and Neelin, 1999). In addition, the Amazon rainforest guarantees fundamental ecosystem services such as food provisioning, biodiversity conservation, climate and freshwater regulation, and natural disaster mitigation (Brandon, 2014; Casagrande et al., 2021; Diaz et al., 2005). The possibility of large-scale disruption of the Amazon ecosystem has attracted public attention in recent decades, mainly due to ongoing human alterations (i.e. deforestation) and anthropogenic climate change (Davidson et al., 2012; Laurance et al., 2012; Malhi et al., 2008). This is explained by the fact that climate influences vegetation functioning and canopy characteristics, but changes in vegetation cover can also modulate climate (Hubbell et al., 2008; Maeda et al., 2015; Nobre et al., 2016). Recent studies have identified changes in the hydroclimatology of the Amazon, particularly in the

* Corresponding author.
E-mail address: sly.wongchuig-correa@univ-grenoble-alpes.fr (S. Wongchuig).

https://doi.org/10.1016/j.jhydrol.2023.130082
Received 27 July 2022; Received in revised form 5 July 2023; Accepted 25 July 2023
Available online 10 August 2023

southern region, where the climate is characterized by strong seasonality, with the dry season becoming longer with anthropogenic climate change, and an intense rate of forest loss documented in the "Arc of deforestation" (Brando et al., 2014; Debortoli et al., 2017; Le Page et al., 2017). Changes in specific hydroclimatic conditions have been related to forest loss, such as precipitation, extension of the dry season, evapotranspiration, among others, which have been found both in observations (Leite-Filho et al., 2019; Wongchuig et al., 2021; Wright et al., 2017) and model experiments (Fu et al., 2013; Lawrence and Vandecar, 2015). While observational studies are essential to confirm past changes, modelling studies allow attributing changes to different drivers, such as forest loss or anthropogenic climate change.

Understanding the mechanisms of water movement both at the surface and in the atmosphere is essential for water resource management practices, flood forecasting and climate projection studies, among others. Impacts in the Amazon hydrological cycle due to land cover changes have been reported to depend on several conditions, such as spatial scales, climate, forest type and hydrological regime (Khanna et al., 2017; Posada-Marín and Salazar, 2022; Rodriguez et al., 2018; Zhang et al., 2017). Some studies, mainly focused on the surface water budget, evaluated the possible effects of climatic variability and land use types (Builes-Jaramillo and Poveda, 2018; Casagrande et al., 2021; Getirana et al., 2014). However, none of them have isolated the sensitivity of the Amazon water budget to changes in land use from other drivers, such as large-scale processes (e.g. global warming). In this sense, a comprehensive description and understanding of the regional or global impacts of deforestation on the water budget requires hydrometeorological modeling systems that represent the processes of the atmosphere, the land surface, and the interactions between them as a coupled system (e.g. coupled General Circulation Models (GCMs), Global Climate Models or Earth System Models (ESMs)) (Davidson et al., 2018; Wagner et al., 2016).

The development of these models prompted the desire to build numerical simulators that would more faithfully represent physical processes, which was made possible by advances in computational resources and simulation techniques (Davison et al., 2018). These models have also been used to simulate the climatic consequences of global deforestation, pantropical deforestation, and regional-scale deforestation in the Amazon basin, respectively (Alves de Oliveira et al., 2021; Avissar and Werth, 2005; Feddema et al., 2005; Lawrence and Chase, 2010).

However, most of the applications performed in the last decades using GCMs have used coarse spatial resolutions (1°–5°) which could hide subregional effects. Usually, these applications of GCMs assume approximations of deforestation scenarios that do not follow a spatially distributed pattern and are therefore unrealistic with current trends, e.g. total Amazon deforestation, etc. This limitation in earlier applications is due to the fact that spatially distributed deforestation scenarios have only become available in recent years (Guimberteau et al., 2017; Lawrence and Vandecar, 2015; Medvigy et al., 2013; Nobre et al., 2009).

In this context, despite the aforementioned studies, no consistent effort has been made to understand/quantify the changes in the components of the water budget in the Amazon due to changes in land use in a spatially and temporally distributed manner. Therefore, this study aims to fill this knowledge gap by analyzing these changes at the subregional level owing the imposition of a more realistic scenario of future deforestation in the Amazon.

The effects of land use changes and interactions with the atmosphere are explored using a regional coupled land–atmosphere model. The experiments discussed here consist of 19-yr simulations for control and deforestation experiments, the latter characterized by a configuration that only modifies land cover maps under a business-as-usual scenario for the year 2050, keeping climatic forcing and boundary conditions the same.

This work is organized as follow: the description of the model, the set-up of the control and deforestation experiment, as well as the data and methods are described in section 2. The section 3 is divided into two parts. First, the validation of the control outputs of the model at the spatial and seasonal level, which will be important to give a degree of confidence to the model simulations for the next analyses, and, second, the analyses and discussions of the changes in the surface and atmospheric water budget components due to deforestation; finally, section 4 presents the conclusions.

2. Material and methods

2.1. Model and experiment set-up

The experiments were simulated using the Regional Earth System Model of the *'Institute Pierre Simon Laplace'* (RegIPSL, https://gitlab.in2p3.fr/ipsl/lmd/intro/regipsl/regipsl/-/wikis/home), which dynamically couples the atmospheric model Weather Research and Forecasting, WRF version 3.7.1 (Skamarock et al., 2008) with the land surface model Organising Carbon and Hydrology In Dynamic Ecosystems, ORCHIDEE, https://orchidee.ipsl.fr/ (Krinner et al., 2005). The WRF model has been widely used for dynamical downscaling in South America (Dominguez et al., 2022; Junquas et al., 2022; Rosales et al., 2022) and for assessing the impact of deforestation on climate (Eiras-Barca et al., 2020; Sierra et al., 2022). The ORCHIDEE model incorporates different hydrological processes that control the dynamics of water over land (modifying the energy balance) as well as the dynamics of rivers and floodplains. ORCHIDEE has also been used to evaluate the dynamics over the Pantanal wetlands (Schrapffer et al., 2020). It also simulates the biophysical and the biogeochemical processes of vegetation that control carbon assimilation by determining the state of the vegetation and its ability to evaporate soil water content (Krinner et al., 2005). This study uses the results of an experiment designed to generate climate data for the South American CORDEX domain (http://www.cordex.org/). The simulation domain covers all of South America with a horizontal resolution of 20x20 km and for the period 2001–2019. The use of a complete continental domain guarantees the representation of all local, regional and interregional climate processes. For instance, processes relevant to spatiotemporal climate variability in the Amazon, such as the South American Monsoon, incursions of southern winds, among others, have been identified (Espinoza et al., 2021; Fu et al., 2013). The spin-up configuration of the experiments is explained in more detail in the supplementary material. Table 1 shows the physical parameterizations used for the atmospheric component of RegIPSL as well as information on the boundary conditions used.

The surface module of the RegIPSL model divides the vegetation into 13 plant functional types (PFTs), which were produced using ESA's CCI Land Cover map (Bontemps et al., 2013). Each PFT follows the same set

Table 1
Parametrization and configuration of the atmospheric component of the RegIPSL model.

Process	Parameterization / configuration	References
Cumulus	Grell Freitas scheme	(Grell and Freitas, 2013)
Surface layer	Mellor–Yamada–Nakanishi–Niino (MYNN)	(Nakanishi and Niino, 2006)
Planetary boundary layer	Mellor Yamada MYNN 2	
Longwave and shortwave radiation	Rapid Radiative Transfer Model for General Circulation Models (RRTMG)	(Iacono et al., 2008)
Cloud microphysics	Morrison two-moment scheme	(Morrison et al., 2009)
Initial and lateral boundary conditions	ERA5	(Hersbach et al., 2020)
Vertical levels	50 levels in the *eta* coordinate system	(Wang et al., 2016)
Large-scale constrain	Spectral nudging	(von Storch et al., 2000)

of equations but with specific parameter values and phenological functions for each PFT (Krinner et al., 2005). PFTs fractions are assigned to different soil tiles, the most relevant in this region being those corresponding to bare soil, short vegetation (grass and crop) and forests (tropical evergreen) (Guimberteau et al., 2018). In the context of evaluating the impacts on the water budget due to changes in land use, two experiments were evaluated in this research. The control and deforestation (hereafter referred to as "2050 deforestation") experiments, which were based on the same configuration, i.e., the same climatic boundary and forcing conditions. However, the 2050 deforestation experiment contemplates a modification of the PFTs based on the projected 2050 deforestation scenario following a "Business As Usual" trend (Soares-Filho et al., 2013). This deforestation scenario has recently been adopted in some research studies (e.g. Abe et al., 2019; Dos Santos et al., 2018; Gomes et al., 2019; Sierra et al., 2022) and assumes the maintenance of the deforestation rates recorded between 1997 and 2002, the non-designation of new protected areas in the basin and the construction of all planned highways (Soares-Filho et al., 2006). For this implementation, pixels from the reference map at 1 km spatial resolution from (Soares-Filho et al., 2013) were added to the PFTs maps at 15 km spatial resolution. Therefore, PFTs maps are interpolated (nearest neighbor remapping) to the model resolution (20 km), ensuring spatial continuity of large-scale vegetation properties, which depend on the new relative distribution of the PFTs at each grid point. Then, the ratio between forest cover and deforested cover for the 2050 scenario was transferred to the PFT maps, for which we assumed a change from category 2 called "tropical broad-leaved evergreen" (hereafter "forest") to category 12 called "C3 crops" (hereafter "cropland"). This means that each pixel of the model PFT (~15 km) the pixels of the deforestation scenario (1 km) from (Soares-Filho et al., 2013) are counted, then the ratio between forest and deforested pixels is calculated. This value replaces the existing crop to forest ratio of the same PFT pixel of the control scenario. For a graphical description of this methodology, see Figure S1. PFT cropland has been chosen over other low vegetation covers (i.e. grass) because it is considered the main driver of forest replacement (i.e. by soybean crops) (Song et al., 2021).

In this RegIPSL model configuration, the PFT maps change every year, following the vegetation dynamics due to current conditions. The PFT maps are therefore imposed because the model is not able to simulate the interaction with the dynamic vegetation. For the 2050 deforestation experiment, the PFTs maps also change each year, but the ratio between the forest and cropland categories is maintained with the 2050 deforested scenario of (Soares-Filho et al., 2013). Fig. 1a shows the maps of land cover fractions or PFTs for the categories changing between the control and 2050 deforestation experiments. For didactic purposes, we have only plotted the year 2010, considered representative of the entire simulation period (2001–2019).

Fig. 1b shows the spatial domain of the simulation covering all of South America, however, given the focus of this study, only the Amazon basin domain (blue polygon) has been considered as a region for the validation analysis (section 3.1). In addition, two other analysis domains were selected. Domain 1, which comprises the entire Amazonian region south of 5°S, is considered for the evaluation of changes in the components of the surface and atmospheric water budget, shown in section 3.2. Domain 2 was chosen to evaluate the particular characteristics of the atmospheric components in a specific region of the deforested patch. More specific analyses were conducted to explain the behavior of surface temperature, specific humidity and winds at all atmospheric levels in relation to land cover change in two cross-sections in the western (cross-section 1) and eastern (cross-section 2) regions of the study area (domain 1), which are plotted in a southwest-northeast direction (see section 3.2.2). The location and direction of these cross sections has been selected because: i) they cover forested and deforested areas, ii) they cover regions located in different parts (west and east) of domain 1, and iii) they roughly follow the predominant climatological wind direction at 850 hPa in this region.

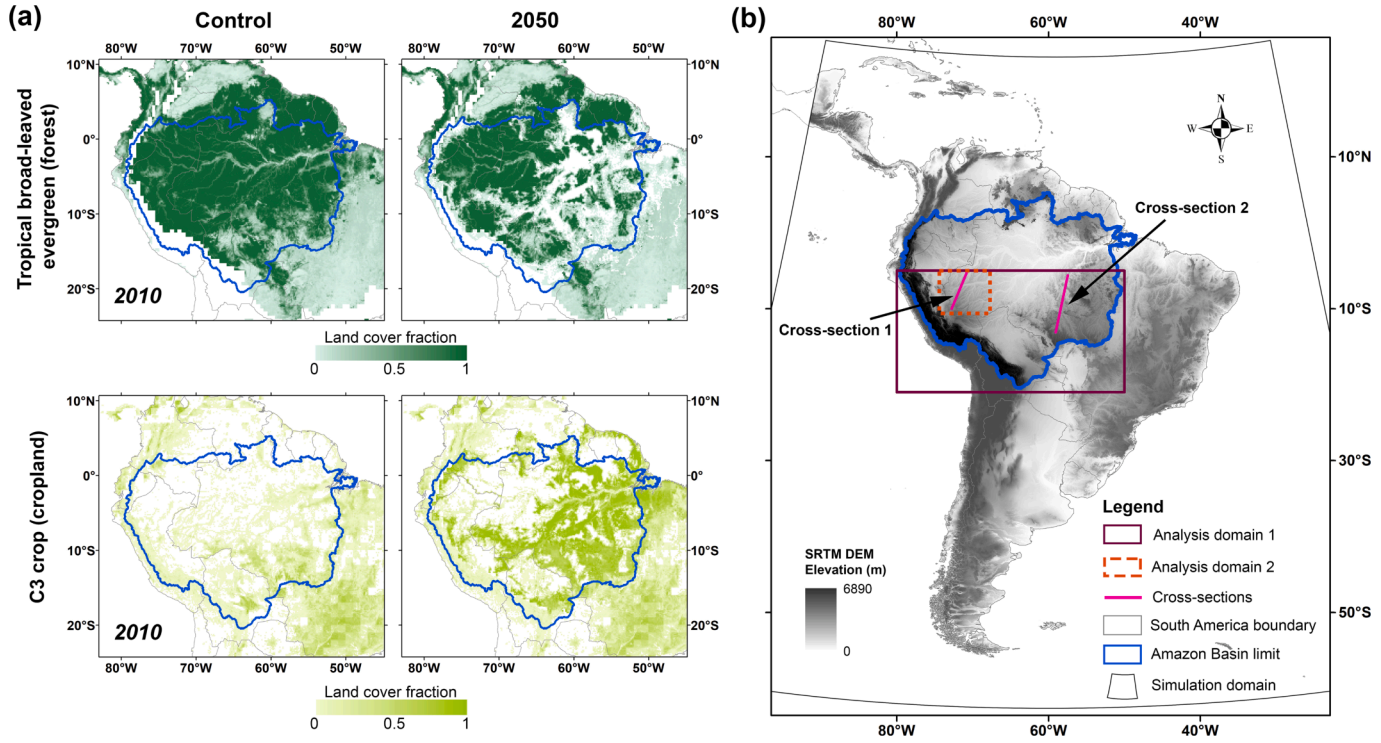

Fig. 1. (a) Land cover fraction maps from 2010 for categories 2 (tropical broadleaf evergreen) for forest and 12 (C3 crops) for cropland of the plant functional types (PFTs) used in the simulations for the control and 2050 deforestation experiments. The latter follows the pathways stated in the LC-14 business as usual scenario for the year 2050 from (Soares-Filho et al. 2013). (b) Simulation and analysis domains covering all of South America and the Amazon Basin, respectively. The relief map from SRTM DEM is in gray scale.

2.2. Datasets for validation and comparison

For the validation of the main components of the surface and atmospheric water budget of the RegIPSL control simulation, numerous hydrological and meteorological datasets based on multiple sources have been selected (see Table 2). Also, data from eight land surface and global hydrological models have been used to compare their actual evapotranspiration outputs. In addition, to discuss the relationships between hydroclimatic components and the deforestation ratio at the observational level for the period 1981–2020, datasets from CHIRPS v2.0 for precipitation, GLEAM for actual evapotranspiration and ESA CCI-LC land cover maps 1992–2020 for deforestation ratio, were specifically used. ERA5 data were used to estimate the moisture flux convergence, to describe the atmospheric water budget and to compare it with the RegIPSL control results.

2.2.1. Actual evapotranspiration

2.2.1.1. Interpolated actual evapotranspiration data (ET-Amazon). The ET-Amazon product, which is based on a fusion of six global evapotranspiration products (GLEAM, SEBS, ALEXI, CMRSET, MOD16, and SSEBop) based on models and remote sensing techniques, was used in this research (Paca et al., 2019). To develop ET-Amazon, seven flux towers from the Large-Scale Biosphere-Atmosphere Experiment in the Amazon (LBA) were used for ground truth validation (Saleska et al., 2013). The ET-Amazon product provides estimates of monthly evapotranspiration rates with a spatial resolution of 250 m for a 10-year period (2003–2013) and is available for the Amazon watershed limits at: <https://www.hydroshare.org/resource/24792a48a6394dcba52da62fa324ae40/>; last accessed October 2021.

2.2.1.2. Land surface and global hydrological models. For a fair and systematic comparison, the eight land surface and global hydrological model datasets from the second eartH2Observe water resources reanalysis (eartH2Observe-WRR2) were used to compare against RegIPSL. These datasets were developed using state-of-the-art modelling systems and provide a robust benchmark for this research. The eartH2Observe global intercomparison project was developed by different institutions for the period 1980–2014 with a spatial resolution of 0.25°. Here we compare the actual evapotranspiration results of a set of models using different equations and therefore a better estimation avoiding individual model's uncertainty (Wartenburger et al., 2018). The models are HTESSEL-CaMa (Bulk formula, (Balsamo et al., 2011)), JULES (Penman-Monteith, (Best et al., 2011; Clark et al., 2011)), LISFLOOD (Penman-Monteith, (Van Der Knijff et al., 2010)), ORCHIDEE (Penman-Monteith, (Barella-Ortiz et al., 2013)), PCR-GLOBWR (Hamon, (Sutanudjaja et al., 2018; van Beek et al., 2011)), SURFEX-TRIP (Penman-Monteith, (Decharme et al., 2013, 2011)), W3 (Penman-Monteith, (van Dijk, 2010; van Dijk et al., 2018)) and WaterGAP3 (Priestley-Taylor, (Flörke et al., 2013; Verzano, 2009)). These datasets are available at: < https://wci.earth2observe.eu/ >; last accessed December 2021.

2.2.2. Precipitation

2.2.2.1. CHIRPS. The Climate Hazards Group InfraRed Precipitation with Station (CHIRPS) data was developed at United States Geological Survey (USGS) and the Earth Resources Observation and Science (EROS) (Funk et al., 2015). CHIRPS v2.0 version was used in this research, which has a spatial resolution of 0.05°x0.05° on a monthly time scale. CHIRPS v2.0 also showed an adequate performance for the Amazon Basin when evaluated against ground-based precipitation stations and in situ discharge observations to represent interannual and multi-decadal variability and interannual trends (Beck et al., 2017; Fassoni-Andrade et al., 2021; Haghtalab et al., 2020; Wongchuig et al., 2017). The dataset is available at <https://data.chc.ucsb.edu/products/CHIRPS-2.0/global_monthly/netcdf/>; last accessed October 2021. Descriptions of the additional precipitation databases that have been considered for this validation (mentioned in Table 2) are described in more detail in the supplementary section.

2.2.3. Terrestrial water storage anomaly

The GRACE (Gravity Recovery and Climate Experiment) dataset was used to validate terrestrial water storage dynamics or variation (dS/dt). This mission was developed by NASA in conjunction with the German space agency German Aerospace Center (DLR), with the purpose of mapping the temporal variations of the earth's gravitational field. In this study, we use three products of equivalent water mass; all based on the last versions of the GRACE v4, but developed by different research centers and laboratories: The Jet Propulsion Laboratory (JPL), the University of Texas Center for Space Research (CSR) and the GeoForschungsZentrum (GFZ) Potsdam. The RL06 (Release-06) data used in this work are CSR, JPL and GFZ data from April 2002 to June 2017 (163-months) and from June 2018 to December 2019 (17-months), from GRACE and GRACE-FO missions respectively, which causes this discontinuity in the data, but which are consistent with each other. The datasets are available at: <https://podaac-tools.jpl.nasa.gov/drive/file

Table 2
List of datasets used for the validation and comparison of the RegIPSL control simulation.

Variable	Product name	Available period	Analysis period	Coverage	Spatial resolution	Temporal resolution	Reference
Precipitation (P)	CHIRPS v2.0	1980-Present	2001–2019	Global	0.05° × 0.05°	Daily	(Funk et al., 2015)
	MSWEP v2.8	1979–2020	2001–2019	Global	0.1° × 0.1°	3–hourly	(Beck et al., 2016)
	TMPA (3B43V7)	1998–2019	2001–2019	50 N to 50S	0.25° × 0.25°	Monthly	(Huffman et al., 2007)
	IMERG (GPM_3IMERGM-V6)	2000–2021	2001–2019	Global	0.1° × 0.1°	Daily	(Huffman et al., 2019)
	HOP	1980–2009	2001–2009	Amazon	1° × 1°	Daily	(Guimberteau et al., 2012)
Actual evapotranspiration (ET)	ET-Amazon	2003–2013	2003–2013	Amazon	250 × 250 m	Monthly	(Paca et al., 2019)
	HTESSEL-CaMa, JULES, LISFLOOD, ORCHIDEE, PCR-GLOBWR, SURFEX-TRIP, W3 and WaterGAP3	1980–2014	2001–2014	Global	0.25° × 0.25°	Daily	(Dutra et al., 2017)
Specific humidity (q), zonal (u) and meridional (v) wind velocity components	ERA5	1979–2021	2001–2019	Global	0.25° × 0.25°, 37 pressure levels	Monthly	(Hersbach et al., 2020)
Terrestrial water storage (TWS) anomaly	GRACE	2002–2021	2002–2019	Global	1° × 1°	Monthly	(Tapley et al., 2004)

s/allData/tellus/L3>; last accessed July 2021.

2.2.4. Specific humidity and horizontal wind components

The 37 atmospheric levels of specific humidity and the zonal and meridional wind components from the ERA5 reanalysis were used to estimate the vertically integrated moisture flux convergence (hereafter called C). We used the re-gridded subset of the full ERA5 data set on native resolution, with a spatial resolution of 0.25°x0.25° and a monthly temporal resolution. The datasets are available at: <https://cds.climate.copernicus.eu/cdsapp#!/dataset/reanalysis-era5-pressure-levels-monthly-means?tab = form>; last accessed February 2022.

C is estimated in this study as the horizontal moisture flux convergence integrated ($-\nabla \bullet (qv)$) between 1000 hPa and 300 hPa (Malik and Taylor, 2011; Rao et al., 1998) for each grid point of RegIPSL and of ERA5. Levels above 300 hPa were not considered because the amount of water vapor is negligible (Strong et al., 2002).

$$-\nabla \bullet (qv) = C = -\frac{1}{g}\int_{p_1}^{p_2}\left(\frac{\partial uq}{\partial x}+\frac{\partial vq}{\partial y}\right)dp \quad (1)$$

where q is the specific humidity, u and v are the zonal and meridional components of the horizontal wind velocity, respectively, p is the pressure and g is the gravitational constant. C is calculated by summarizing the horizontal moisture flux convergence over the intervals of pressure levels using finite centered differences on a latitude-longitude grid point, between pressure level of 1000 hPa for p_1 and higher level at 300 hPa for p_2.

Fig. 2 shows the flow diagram of the main components of the surface and atmospheric water budget, together with the datasets that have been used for the validation and comparison of each of them. These components are precipitation (P), actual evapotranspiration (ET), runoff (R), terrestrial water storage variation (dS/dt), vertically integrated moisture flux convergence (C) and precipitable water variation (dW/dt). Note that the terms R and dW/dt were not validated, mainly because we preferred to use as much as possible observation-based and spatially distributed datasets, e.g. the R observations are given as an aggregation at the catchment level and would not be available in a gridded form, as is being analyzed in this study. Details on validation results of the dS/dt and C are shown in the supplementary material.

2.3. Performance metrics for validation

The following performance metrics are used in this research for validation on a monthly scale in a spatially distributed manner i.e. for each grid point. Some results are shown as the aggregation of these metrics from grid points belonging to regions such as north and south of 5°S for example. The bias measures the temporal average tendency of the simulated data to be higher or smaller than observed variables (Gupta et al., 1999; Singh et al., 2005). The Kling-Gupta Efficiency (KGE) is a statistic index proposed by (Gupta et al., 2009) and modified according (Kling et al., 2012), it uses most aspects such as correlation, variability (standard deviation) and relative bias terms (means).

$$BIAS(\%) = \frac{\sum_{i=1}^{nt}(V_{sim}(t)) - \sum_{i=1}^{nt}(V_{obs}(t))}{\sum_{i=1}^{nt}(V_{obs}(t))} \bullet 100\% \quad (2)$$

$$KGE = 1 - \sqrt{(r-1)^2 + \left(\frac{\sigma sim/\mu sim}{obs/\mu obs}\right)^2 + \left(\frac{\mu_{sim}}{\mu_{obs}} - 1\right)^2} \quad (3)$$

where nt is the number of observations. The r is the Pearson linear correlation coefficient between simulated and observed variable, σ and μ are the standard deviation and the mean respectively. The KGE index range between -∞ and 1 (perfect fit).

For the monthly time series of terrestrial water storage variation (dS/dt)) the Nash–Sutcliffe efficiency (NSE) (Nash and Sutcliffe, 1970) was also assessed. To compute temporal trends of hydroclimatic variables over the last four decades, we assess the rank-based non-parametric Kendall test (Kendall, 1975). For this study, the significance of statistical tests is evaluated at 95% ($p < 0.05$).

2.4. Analysis of the hydroclimatological components related to the deforested patch

Calculations of the surface and atmospheric water budget components were performed for "domain 1" (Fig. 1b), which corresponds to the Amazon region south of 5°S and below 1,000 m a.s.l, to exclude the mountainous regions from the analysis. These analyses are presented in section 3.2.

The percentages of PFT changes from forest to cropland (deforestation) are computed based on the concept of buffer zones, which

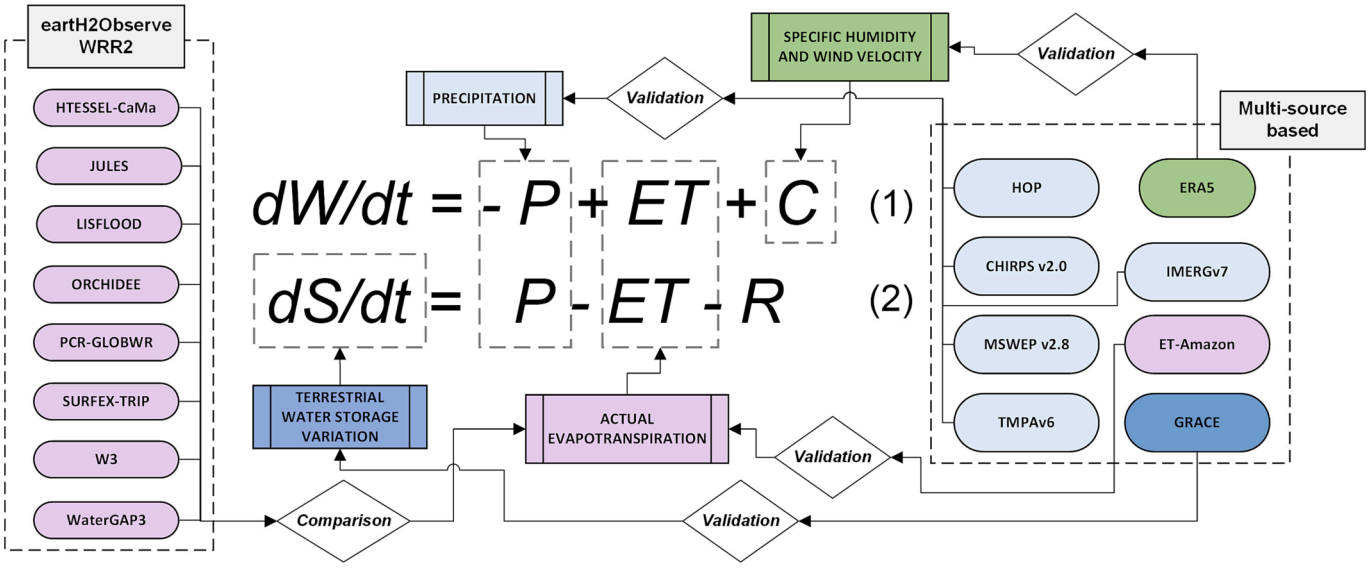

Fig. 2. Flowchart of the datasets used to validate and compare the main components of the (1) atmospheric and (2) surface water budget equations applied to each grid point and on a monthly scale. Precipitation (P, sky blue), actual evapotranspiration (ET, violet), terrestrial water storage variation (dS/dt, blue) and vertically integrated moisture flux convergence components (C, green). (For interpretation of the references to color in this figure legend, the reader is referred to the web version of this article.)

corresponds to the ratio of deforested PFTs grid points within the neighborhood surrounding 50 km radius of influence around each RegIPSL grid point. This value of the radius of influence has been estimated in previous studies as adequate in terms of sensitivity between deforestation and hydroclimatic components (Debortoli et al., 2015; Wongchuig et al., 2021).

A spatial analysis was also performed, relating significant changes at each grid point of atmospheric components such as C and dW/dt to the spatial proximity to the nearest edge of the deforested patch. These results are specifically shown in subsection 3.2.2.

3. Results and discussions

In this section we show and discuss two main results 1) the validation of many variables of the RegIPSL model that will be important in terms of model reliability for the analyses of the second part on 2) the evaluation of the impacts of deforestation on the main components of the surface and atmospheric water budget.

3.1. Model validation

Fig. 3a shows the maps of the annual mean climatology for the RegIPSL control experiment and CHIRPS dataset for the period 2001–2019. Both show highest P amounts for the southeastern (south of 8°S) Andean region, as well as both are able to identify "rainfall hotspot" at the east flank of the Andes, where P can reach values of 6,000 mm year^{-1} (Espinoza et al., 2015). Regions located above 1,000 m a.s.l. were not considered for the analysis in this research to avoid the complex topography and steep slopes areas (greater than15%, see Fig. S2) that affect convection (Wongchuig et al., 2021), and therefore show a high relative bias especially in the Andean region of Peru and Bolivia. In addition, in general terms, the best performance considering the Kling-Gupta Efficiency index, the model performs best in domain 1. The mean values using all databases compared to RegIPSL are 0.3 and 0.6 for the regions north and south of 5°S, respectively.

Looking at the seasonal variability, RegIPSL underestimates P compared to the CHIRPS (Fig. 3c), during the austral summer (December-March) in both the northern and southern 5°S region. In the southern 5°S region, P is in agreement with the observational series during the dry period (May to September). The other precipitation databases show similar performance to each other and are presented in the supplementary material.

For the validation of the monthly ET, only a multi-source database (ET-Amazon) for the period 2003–2013 was used (Fig. 4). Considering the annual climatology, the RegIPSL simulation follows a similar spatial pattern to the ET-Amazon reference, with lower values in the Andes region and in the southern Amazon region. However, the lowest statistical performance indices were also found in these regions (Fig. 4a).

Considering that the eight land surface and global hydrological models still have some uncertainty in representing ET (~20% bias and 0.26 KGE), it is remarkable that the RegIPSL has an agreement of ~3% and 4.6 for bias and KGE, respectively, when evaluated against ET-Amazon, mainly in the region south of 5°S, with a slight underestimation during the dry period (May to September) (Fig. 4c). In addition, the envelope of the eartH2Observe-WRR2 outputs compared to the ET-Amazon base shows a greater dispersion of ET at the seasonal climatology level for both the northern and southern 5°S region.

The results of the RegIPSL model performance in the southern Amazon (south of 5°S) which belongs to the study area (domain 1) indicate that, according to the bias and KGE statistical indices, the values for P (ET) are ~4% and 0.6 (~3% and 4.6), respectively. This can be considered adequate for a monthly and continental scale analysis to be performed in this study, considering the lower performance of the global model outputs used for ET and global product bias values for P that are around ~10–15% for the study region (Beck et al., 2017).

Validation of other water budget components is described in detail in the supplementary material. In summary, the RegIPSL performance of the terrestrial water storage variation (dS/dt) shows a bipolar bias contrast between the northeast region and the rest of the Amazon, during the transition periods (MAM and SON). Considering the vertically integrated moisture flux convergence (C) components, RegIPSL shows a systematic underestimation in the western region of the Amazon basin, which is reflected in the low values of KGE. In general, both dS/dt and C had better statistical performance in the region south of 5°S compared to the north, considering the bias and the NSE indices.

It should be noted here that, according to many studies, long-term water budget using datasets (e.g. observations) from different sources may result in non-closure of the balance (imbalance), which is mainly due to the different uncertainties of each source and the combination of different variables. According to (Costa et al., 2021, p. 20) many studies that have evaluated the water budget in the Amazon (e.g. Builes-Jaramillo and Poveda, 2018; Carmona Duque 2015; Getirana et al. 2014; Marengo et al., 2004; Salazar Villegas et al. 2006) have estimated, based on different sources, different degrees of uncertainty for different components. For instance, annual averages for P are ~2190 mm yr^{-1} ± 7% and a much larger uncertainty for ET is ~1250 mm yr^{-1} ± 50%. When the imbalance was calculated by (Builes-Jaramillo and Poveda, 2018) at the atmospheric level (P-ET-C), an average value was estimated from different studies of the last decades in the Amazon of 191 mm yr^{-1} (~0.52 mm day^{-1}). This means that the imbalance in the closure of the Amazon atmospheric water cycle with the data bases to date is of that order of magnitude and is considered in this work also as an uncertainty benchmark when analyzing and discussing the observed data at the end of section 3.2.2.

3.2. Hydroclimate changes induced by deforestation

3.2.1. Changes in the surface water budget

Fig. 5 shows the differences between the 2050 deforestation and control experiments for seasonal P. Temporally significant increases in P (bright blue dots) are observed mainly in the SON and DJF periods (Fig. 5a), which represent the rainy season in the study region (domain 1). In addition, we wanted to see how significant differences in these variables are spatially distributed and thus how they relate to deforested areas. Fig. 5b shows remarkably that, in general, significant positive changes in P grid points (black dots) occur to a greater extent in regions associated with deforestation values above 40% (for deforestation ratio estimates, see section 2.5). While significant decreases in P (bright red dots) have been recorded mainly in the DJF and MAM periods in the northeastern region of domain 1 and in areas surrounding the deforested patch.

We also plotted the frequency distribution of the grid points (violin plots, the area of which adds up to 1) with significant increases (decreases) in blue (red) distribution and the non-significant ones (gray distribution). It should be noted that the vertical axes of the violin plots have a separate scale for significant and non-significant grid points. This scale allows to have a visual representation of the percentage of grid points (e.g. positive or negative, significant or non-significant) relative to the total study area. This type of graphs allows a clear visualization of how grid points with a difference in P are distributed in relation to their associated percentage of deforested area. To characterize and quantify these differences, the median and the standard deviation of each distribution (e.g. for significant positive grid points) were estimated. Grid points representing significant increase values have, on average for all seasons, a median (standard deviation) of 60% (18%), while the grid points with non-significant changes have values of 36% (26%) of the deforestation ratio. Significantly positive grids are preferentially aggregated in regions with deforestation values above 40% that occur mainly during the SON period. Regarding other seasons, few significant changes in P are detected and a mean annual change of about 47- and 10-mm year^{-1} is computed for the average of grid points inside and outside the deforested patch, respectively, with significant changes

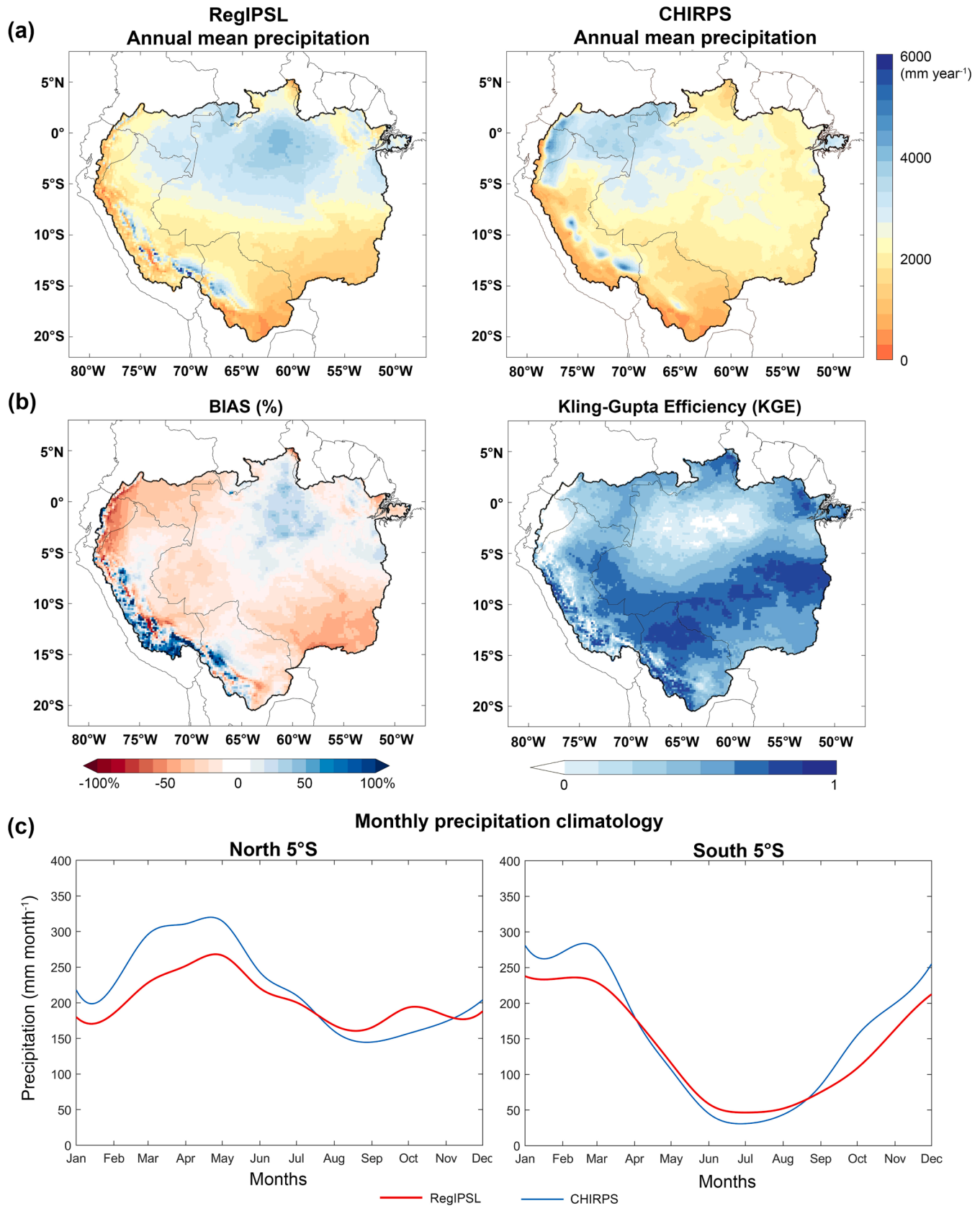

Fig. 3. (a) Annual precipitation climatology from RegIPSL simulation and gridded CHIRPS dataset for the period 2001–2019. (b) Maps of the BIAS and KGE indices between RegIPSL and CHIRPS for the monthly series during the period 2001–2019. (c) Time series of monthly precipitation climatology for RegIPSL and CHIRPS precipitation dataset for the regions north and south of 5°S and for areas below 1,000 m a.s.l.

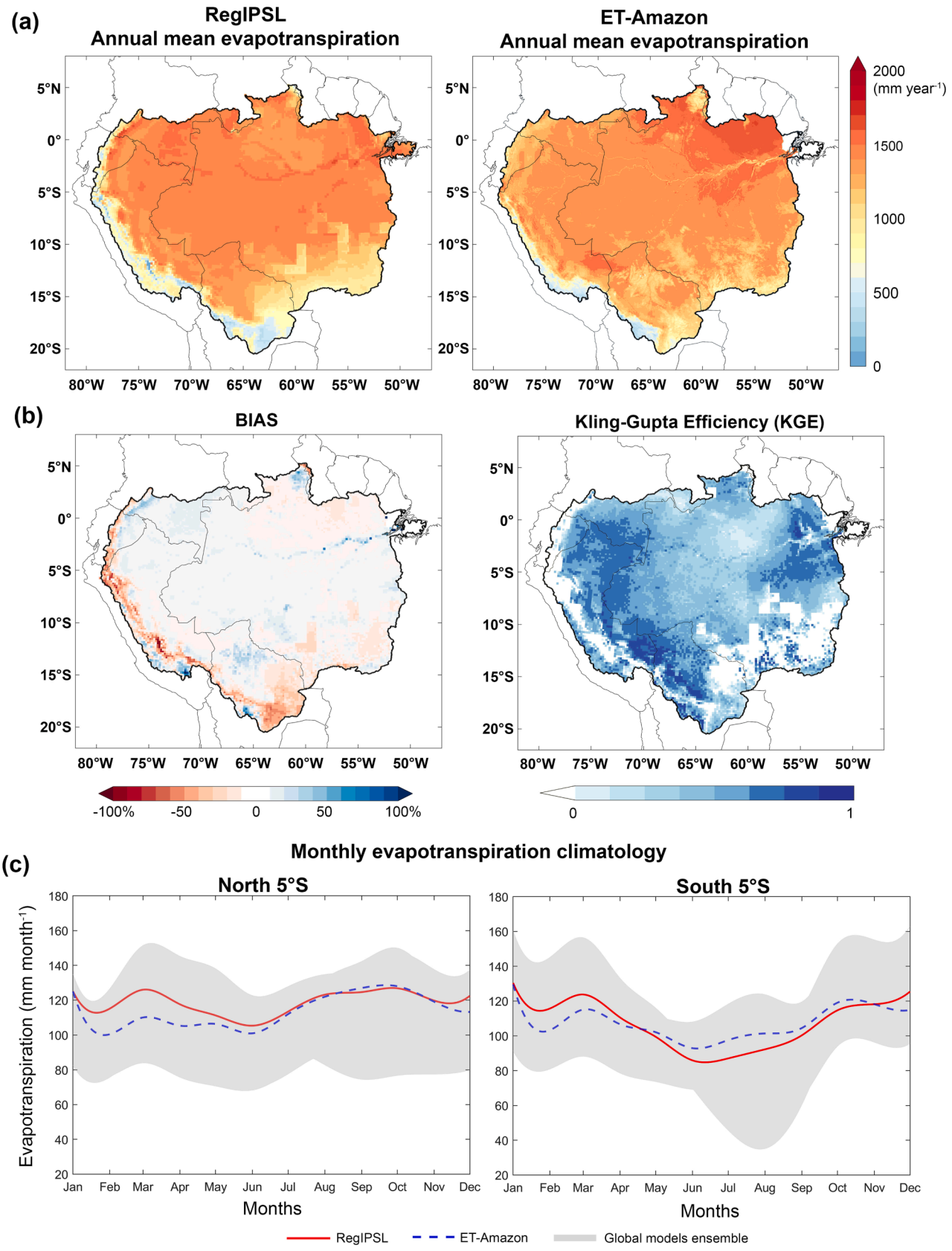

Fig. 4. (a) Annual actual evapotranspiration climatology from RegIPSL simulation (2001–2019) and gridded observed ET-Amazon data set (2003–2013). (b) Maps of the BIAS and KGE indices between RegIPSL and ET-Amazon for the monthly series during the common period 2003–2013. (c) Time series of monthly actual evapotranspiration climatology for RegIPSL, ET-Amazon dataset and land surface and global hydrological model's ensemble envelope in gray for the regions north and south of 5°S and for areas below 1,000 m a.s.l.

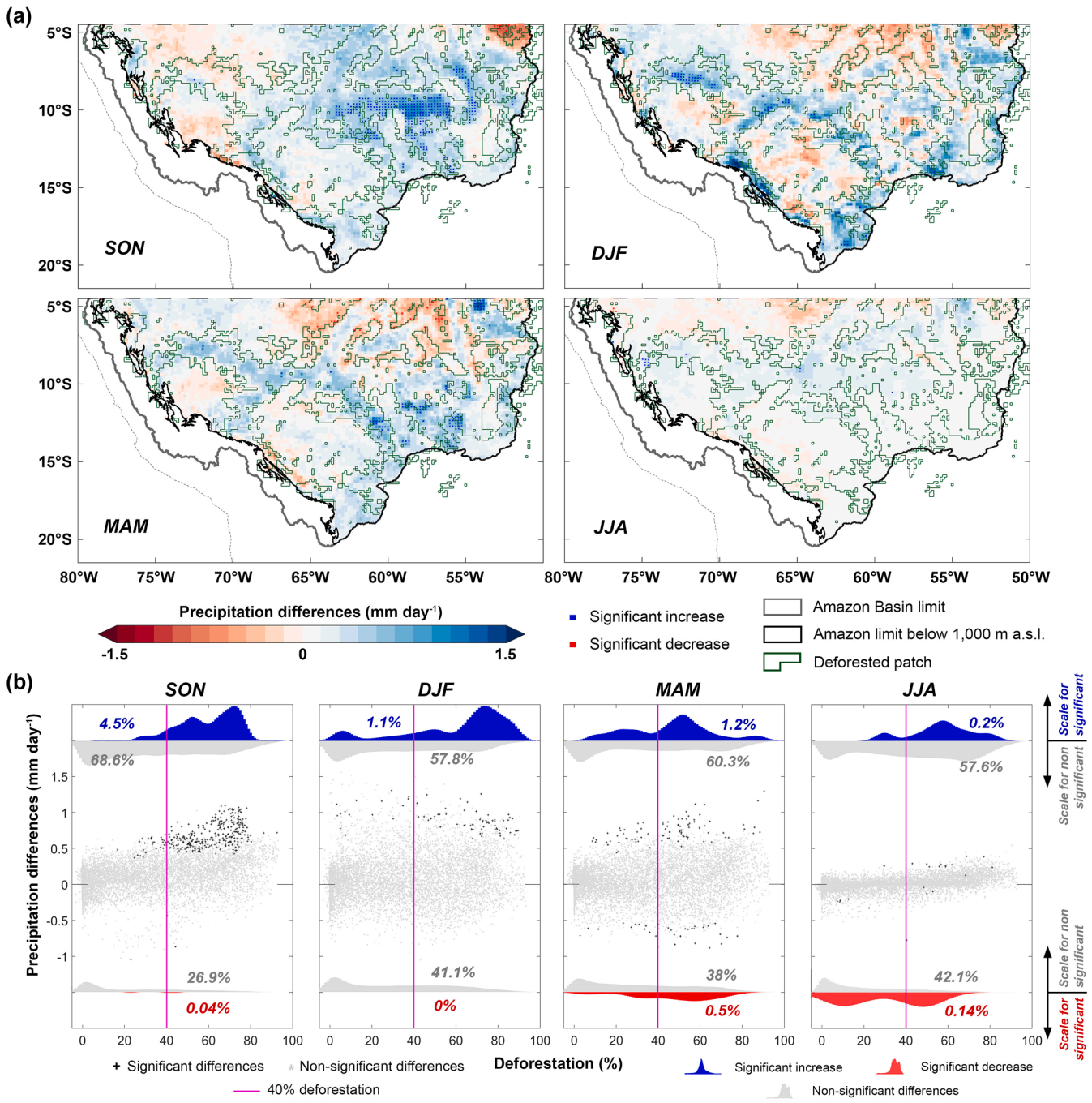

Fig. 5. (a) Maps of precipitation differences between the deforested and control experiments in red to blue color scale. Grid points with significant differences show a red or blue dot for decrease or increase, respectively. (b) Differences in precipitation between the 2050 deforestation and control experiments, by season and its relationship with the percentage of deforestation. The grid points with significant differences are presented as crosses in black color and their probability of precipitation increase (decrease) distribution is shown in blue (red) color in a violin plot, while non-significant variations are shown in gray color. The percentages indicate the proportion of grid points in relation to the total. (For interpretation of the references to color in this figure legend, the reader is referred to the web version of this article.)

occurring only inside the patch. Decreases in P are significantly smaller in number of grid points and with a larger spread along the entire x-axis (deforestation) compared to significant increases.

Fig. 6a shows that ET decreases systematically in virtually the entire deforested patch, mainly during the dry season (JJA) and the beginning of the wet period (SON), which is likely due to largest changes in energy partitioning toward an increase in sensible heat flux (see Fig. S7 in supplement) resulting in warmer surface temperatures, mainly within the deforested patch (see section 3.2.2). This could also be impacting the availability of water in the soil (see Fig. S8). Specifically, during the SON period, a dipole can be observed for ET changes in the central-eastern region of domain 1, with decreases associated with regions within the deforested area and increases preferentially on the southern edges. This dipole behavior can also be observed in surface temperature and low-level cloudiness changes (see section 3.2.2). Fig. 6b shows that grid points with significant values of decreasing ET (black dots) are associated with high values of deforestation ratio (greater than40%), more noticeable during JJA and SON. When analyzing the statistics of the distributions (not shown) the significantly negative grid points have a lower dispersion (low standard deviation) compared to the non-

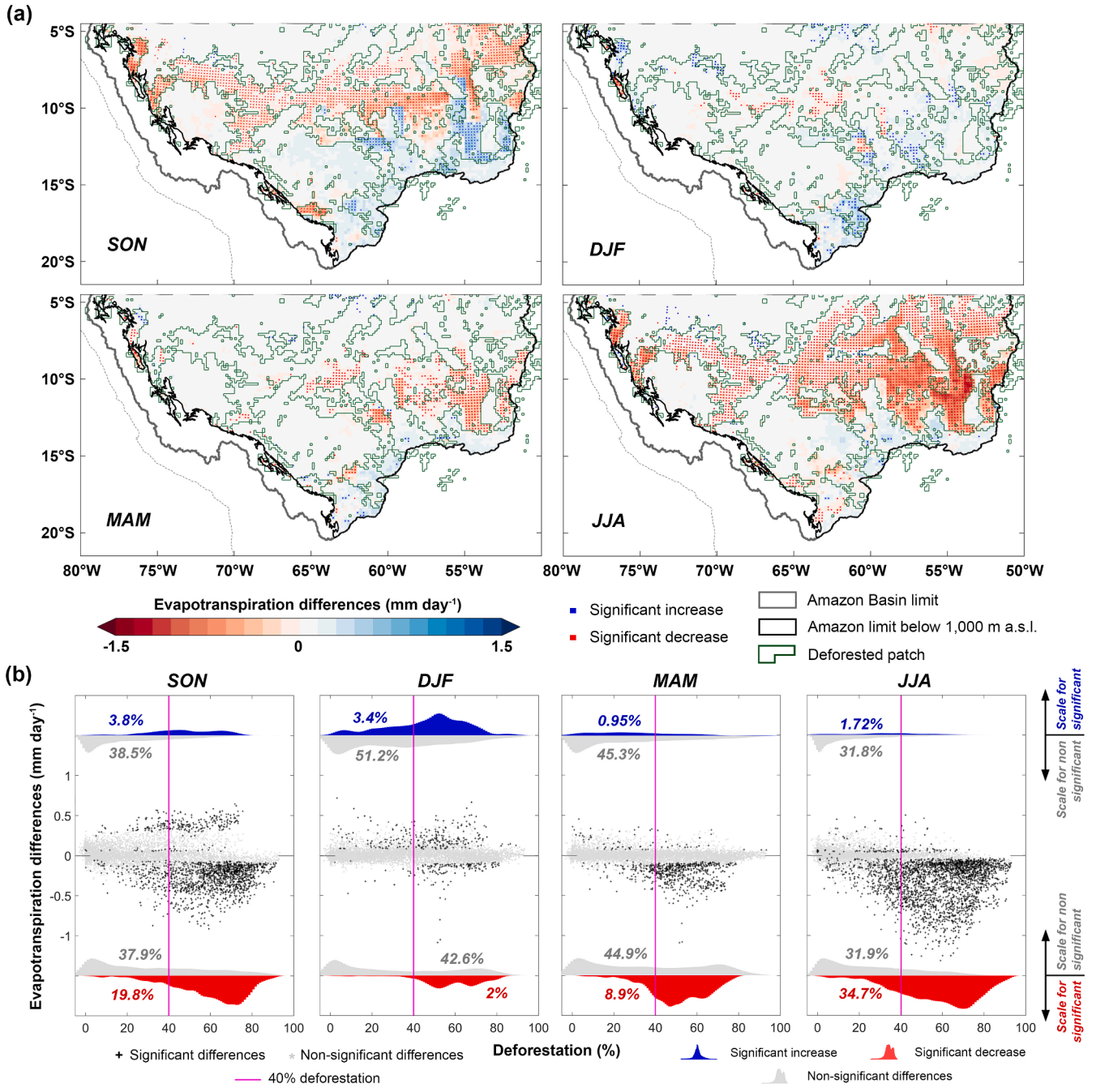

Fig. 6. (a) Maps of actual evapotranspiration differences between the deforested and control experiments in red to blue color scale. Grid points with significant differences show a red or blue dot for decrease or increase, respectively. (b) Differences in actual evapotranspiration between the 2050 deforestation and control experiments, by season and its relationship with the percentage of deforestation. The grid points with significant differences are presented as crosses in black color and their probability of evapotranspiration increase (decrease) distribution is shown in blue (red) color in a violin plot, while non-significant variations are shown in gray color. The percentages indicate the proportion of grid points in relation to the total. (For interpretation of the references to color in this figure legend, the reader is referred to the web version of this article.)

significant ones.

Observations have also identified a significant sensitivity of P and ET to high ratio of deforestation (particularly close to 40%). First, a value of 40% deforestation has been estimated as a possible threshold for a point of no return ("tipping point") of conversion of the Amazonian tropical forest to a new state with savanna-like conditions (Nobre et al., 2016; Nobre and Borma, 2009), and secondly, for example, by (Wongchuig et al., 2021) when analyzing P and ET trends associated with the percentage of deforestation using observations. This pattern has also been corroborated by extending this analysis for the period 1981 to 2020 using observed CHIRPS and GLEAM data (see Figs. S9 and S10), where it is shown that only grid points associated with deforestation values above 40% show significant decreasing trends. This is contrary to what was found in this study for P, which significant upward trend is associated with a higher deforestation ratio.

The seasonal spatial patterns of surface runoff (R) differences are shown in Fig. 7b. It is important to realize here that changes in PFTs in ORCHIDEE do not change soil properties (e.g. soil compaction, biomass wash-out, among others), therefore changes in runoff generation due to changes in infiltration, for example, would be due to variations in

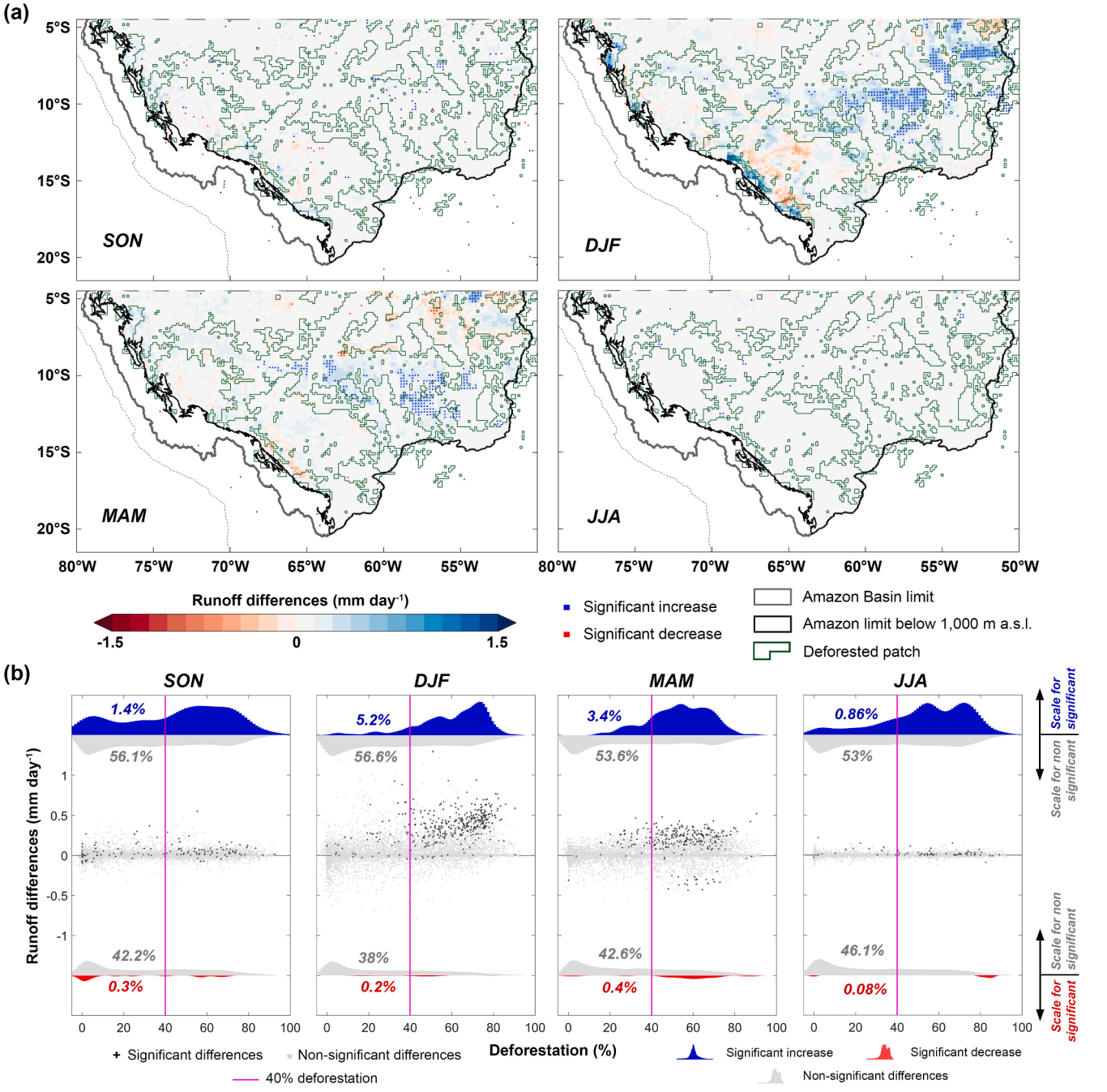

Fig. 7. (a) Maps of runoff differences between the deforested and control experiments in red to blue color scale. Grid points with significant differences show a red or blue dot for decrease or increase, respectively. (b) Differences in runoff between the 2050 deforestation and control experiments, by season and its relationship with the percentage of deforestation. The grid points with significant differences are presented as crosses in black color and their probability of runoff increase (decrease) distribution is shown in blue (red) color in a violin plot, while non-significant variations are shown in gray color. The percentages indicate the proportion of grid points in relation to the total. (For interpretation of the references to color in this figure legend, the reader is referred to the web version of this article.)

available water in the soil and/or due to changes in precipitation. The results show that there is a slight increase in runoff generation during the wet period (DJF), which is mainly a consequence of P increases and ET decreases in the previous season (SON) (Figs. 5 and 6). The decreases in ET are keeping the three soil layers represented by ORCHIDEE (de Rosnay and Polcher, 1998) with a greater amount of water, causing an increase in runoff when rainfall events occur; these significant increases in P occur in the east-central region of domain 1 (east of 65°W) within the deforested patch and during SON and DJF seasons. Significant increases in R occur particularly in regions with a percentage of deforestation greater than 40% (Fig. 7b) and mainly during the peak of the wet season (DJF). This is in agreement with studies in the Amazon that, in general, observed an increase in discharge when deforestation occurs, some considering feedbacks between the surface and the atmosphere (e.g. (Guimberteau et al., 2017; Stickler et al., 2013; Weng et al., 2018). However, this region (east of 65°W) belongs to the steepest areas of the lower Amazon (see Fig. S2), which may have further triggered runoff generation when there is an increase in surface water as occurs during the onset of the rainy season (between SON and DJF).

As the last term of the surface water budget, the variation of water that remains stored in all soil layers is analyzed. Fig. 8 shows that dS/dt increases mainly within the deforested patch, associated with changes in

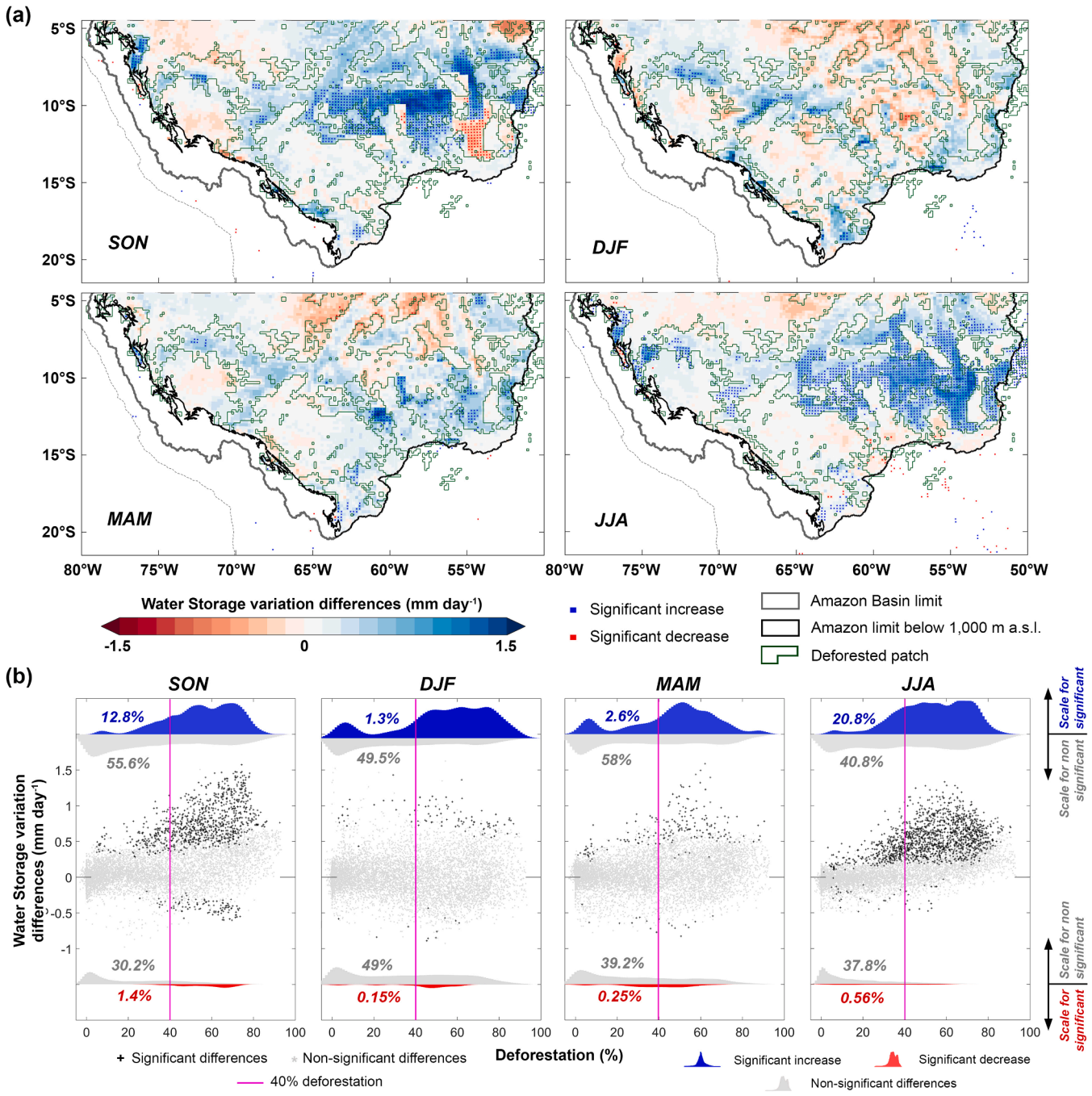

Fig. 8. (a) Maps of water storage variation differences between the deforested and control experiments in red to blue color scale. Grid points with significant differences show a red or blue dot for decrease or increase, respectively. (b) Differences in water storage variation between the 2050 deforestation and control experiments, by season and its relationship with the percentage of deforestation. The grid points with significant differences are presented as crosses in black color and their probability of water storage variation increase (decrease) distribution is shown in blue (red) color in a violin plot, while non-significant variations are shown in gray color. The percentages indicate the proportion of grid points in relation to the total. (For interpretation of the references to color in this figure legend, the reader is referred to the web version of this article.)

ET, R and root zone moisture (see Figs. 6, 7 and supplement). Note that during SON the soil root zone has already increased its moisture, therefore when the wet season starts in DJF, this triggers the increase in runoff in this season because the soil is already saturated. Considering the relationship between changes in dS/dt with changes in ET, they are highly anti-correlated (r = -0.62), as can be observed spatially and temporally among seasons, mainly within the deforested patch (Fig. 6a and 8a). This pattern could be explained by the reduction in ET, i.e., existing soil water is evapotranspired at a lower rate in the 2050 deforestation experiment than in the control, which have access to a deeper root zone. Thus, in the 2050 deforestation experiment, an increase in water availability in the soil root zone is evident (see Fig. S8). This behavior also extends to the spatial level associated with the percentage of deforested areas, i.e., significant increases in dS/dt occur at grid points associated with deforestations above 40%, mainly during SON and JJA (Fig. 8b).

3.2.2. *Changes in the atmospheric water budget*

In this subsection, the results of the atmospheric components of the water budget (in addition to P and ET) are analyzed and discussed. These

are the vertically integrated moisture flux convergence (C) between the 1,000 and 300 hPa levels, as well as the precipitable water variation (dW/dt). Our analysis shows that during the SON season, C increases significantly (blue dots in Fig. 9a), particularly in the southern region of the deforested patch, which is oriented downwind of the winds at 850 hPa (gray and black arrows) during that period. Decreases in C (red dots) are located mainly in the windward region of the deforested patch, which can be seen most clearly in the rectangle of dashed lines in the western region of our analysis area (domain 2 in Fig. 1 and Fig. 9a). It has been observed that the grid points with significant differences (decrease or increase) in C are associated with values closer to the deforested edge, mainly in the SON period, which corresponds to the phenomenon observed by (Khanna et al., 2017) regarding a suppression of convection in the upwind sector while convection increases downwind. The distance of grid points to the nearest edge of the patch was considered as positive (negative) values for grid points located outside (inside) the patch. In the east-central region, significant wind increases (black arrows) are observed at 850 hPa in a southwesterly direction

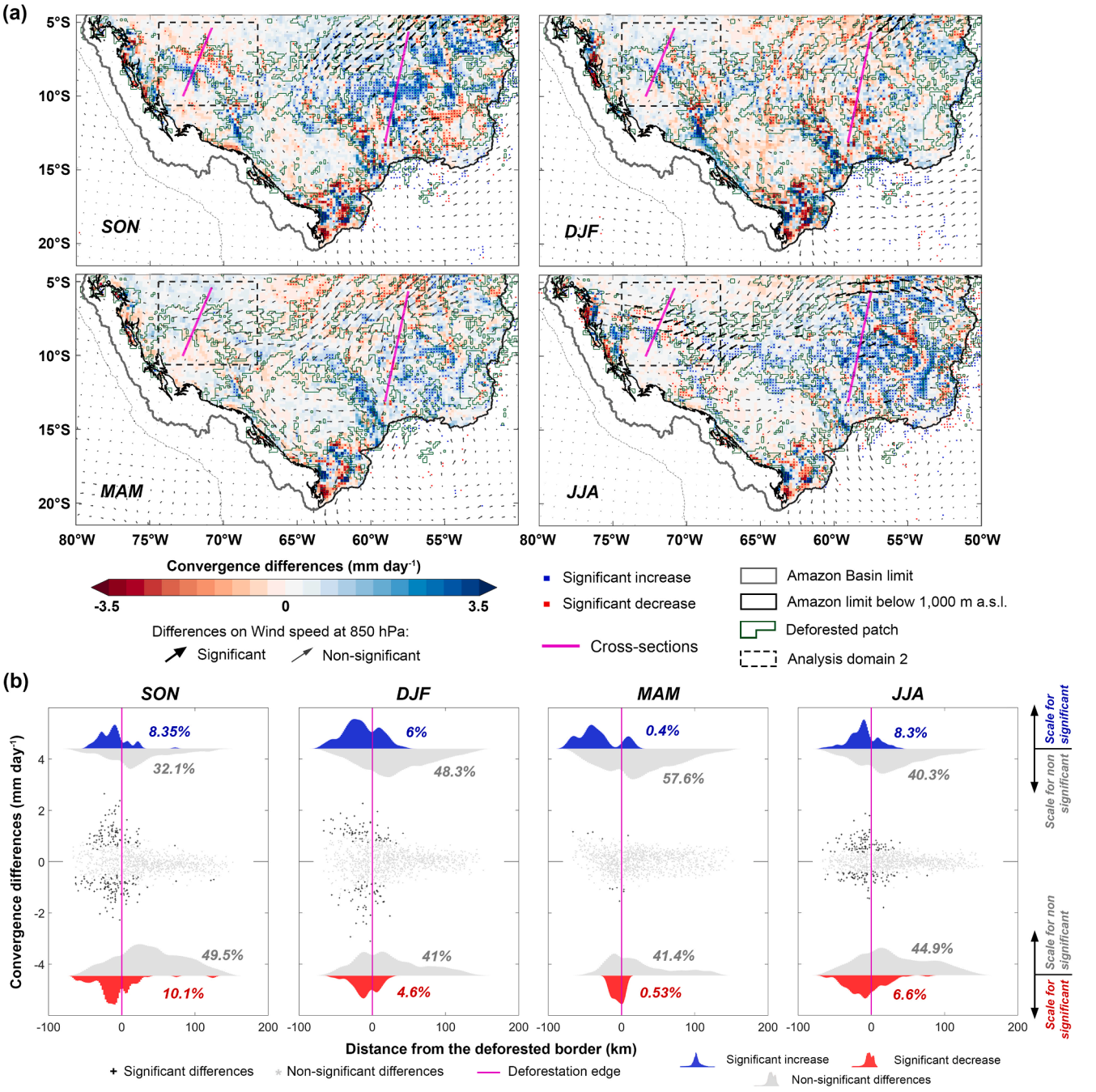

Fig. 9. (a) Maps of convergence differences between the deforested and control experiments in red to blue color scale. Grid points with significant differences show a red or blue dot for decrease or increase, respectively. The dashed rectangle represents domain 2 and magenta lines are the cross-sections 1 and 2. The difference in wind speed at 850 hPa are plotted as black and gray arrows for significant and non-significant values, respectively. (b) Differences in convergence between the 2050 deforestation and control experiments, by season and its relation to the distance to the edge of the deforested patch. For the analysis domain 2 (dotted rectangle), the grid points with significant differences are presented as crosses in black color and their probability of convergence increase and decrease distribution is shown in blue and red color in a violin plot, respectively, while non-significant variations are shown in gray color. The percentages indicate the proportion of grid points in relation to the total. (For interpretation of the references to color in this figure legend, the reader is referred to the web version of this article.)

during the SON period, which cross the deforested patch and ends in the region with a significant increase in surface temperature (not shown) producing moisture convergence. This convergence would be triggering convection and precipitation in this region as it encounters a warmer surface (thermal processes) as substantiated by (Khanna et al., 2017).

Once C is analyzed spatially, this helps us explain changes in P. For instance, many previous studies have described significant increases in P during the SON and DJF periods, indicating that the intertropical convergence zone (ITCZ) is quite sensitive to land surface changes (Feng and Fu, 2013; Lau et al., 2020). During SON, P increases occur in the east-central region, possibly due to increased moisture transport brought by northeasterly winds in this region (see Fig. 9), which encounter a warmer surface (not shown) triggering convection in this region. During the wet season (DJF), increases in P occur in the southern region of the deforested patch (green polygon), which would correspond to the leeward region. This occurs due to a phenomenon modelled by (Khanna et al. 2017), whereby the decrease in surface roughness results in a suppression of convection in the upwind sector while convection increases in the downwind oriented sector of the deforested patch.

A more detailed analysis of the humidity fluxes during the periods with the most significant changes (SON and DJF) in the Amazon region south of 5°S is performed. Fig. 10 shows cross-sections 1 and 2 with the differences of the specific humidity and the horizontal and vertical wind components plotted between the 200 and 1,000 hPa levels. To plot the winds shown as black arrows, the horizontal U and V components were decomposed into a component parallel and a component perpendicular to the coordinate system of each cross section. Finally, this parallel component and the original vertical component W were used as the new horizontal and vertical components, respectively, of the cross-sectional plane. The upper bar corresponds to the height of the Planetary boundary layer (PBL). Differences in surface temperature, roughness length and soil root zone moisture are shown in the lower bars along with regions with forested or cropland areas.

The increase in surface temperature has been recorded mainly in the center of the deforestation pathway, while the decrease is more associated with the regions near the deforested edge (not shown). However, this increase, as seen in the cross-sections in Fig. 10, has been evident in the downwind (southwest) oriented regions of the deforested patch. Also, at the surface level, there is a systematic pattern for all season with significant increase in soil moisture occur in the southwestern region of the deforested patch (Figs. S8 and 10). This is due to the consistent effects of the other components of the surface water budget, having a similar spatial pattern to dS/dt (see Fig. 8).

In cross-section 1, the deforestation pathway is about 350 km, which is considered here as "medium-size" pathway considering, as a reference, the study of (Khanna et al., 2017) in which the Rondônia region studied had a size of about 200 km. During the SON season (Fig. 10a left column), the same pattern discussed above occurs with respect to P and C, in which reductions in surface roughness length due to deforestation result in a suppression of convection in the upwind sector, while convection increases in the downwind oriented sector of the deforestation pathway, revealing the emergence of a dipole (see Fig. 9a and 11a). This effect has been suggested and documented by (Khanna and Medvigy, 2014), where horizontal variations in surface roughness length between deforested patches (sparse low vegetation) and rough forests, which are less aerodynamic, may lead to a spatial redistribution of precipitation that is not explained solely by thermal processes. In cross-section 1 during the SON period, there are also increases in surface temperature and locally higher moisture fluxes that are generated mainly at the 750 hPa level over the downwind oriented sector (southern part) of the cross-section. It is precisely in this area where P increases (see Fig. 5a) and where we find more cloudy conditions at low levels (clouds below 680 hPa; not shown). Nevertheless, surface cooling occurs in the upwind sector (northern part) of the cross-section 1, decreasing the PBL height in the deforested conditions and concentrating atmospheric moisture at the bottom of the troposphere near 1000 hPa levels (see Fig. 10a). A shallower PBL in the northern part of cross-section 1 reflects the more stable conditions in this area. During DJF, the areas where the most significant increase in P is located in cross-section 1 also show a significant increase in atmospheric moisture at low levels (~975 hPa). The significant decrease in surface temperature occurs over the deforested area at this season, leading to a shrinking of the PBL and an increase in atmospheric humidity near the surface (between 800 hPa and 900 hPa).

For cross-section 2, which is located in the east-central region of analysis domain 1 (see Fig. 1), the deforestation pathway can reach large extensions of ~500 km (considered here as a "large-size" pathway). The orientation of this cross-section has been chosen because it is parallel to the wind direction climatology and because it occupies the longest and continuous deforestation pathway in the 2050 deforested scenario patch. During the SON period, which is when the largest area of significant precipitation increase occurs (see Fig. 5), the increase in specific humidity occurs at different levels, enhancing the probability of precipitation generation. It is interesting to note that the increased atmospheric moisture near the downwind edge of the deforested patch appears to be caused by higher precipitation falling in this area, while the wetter lower troposphere in the northern part is caused by a shallower PBL driven by cooler surface temperatures (see Fig. 10a). Atmospheric moisture increases develop at two different altitudes: one of them at 750 hPa located in the center of the deforested patch. In this region the surface temperature increases and the PBL undergoes small altitude changes and low-level cloud growth. The other altitude is located at ~975 hPa mainly downwind of the deforested patch, which is related to a lower PBL and more stable atmospheric conditions. This pattern is interesting because it is a combined effect of the dominant convection processes at different scales of the deforestation pathways with a greater dominance of the roughness effect over the thermal effect due to the larger scale of deforestation in cross-section 2 (Avissar and Schmidt, 1998; Patton et al., 2005).

Finally, we analyze the variation of precipitable water (dW/dt), i.e. how much water remains in the atmosphere. The results show that although C increases during most of the year in the deforested patch (see Fig. 9), the increase in P and the significant decrease in ET cause the dW/dt in the atmosphere to decrease (Figs. 11 and 12), i.e., the atmosphere becomes drier in the deforested patch. This particular phenomenon can also be identified by observations of current deforestation conditions (1992–2020) (see Fig. S11). The uncertainties in the atmospheric imbalance based on the literature review (Builes-Jaramillo and Poveda, 2018), which is around the value of 0.52 mm day^{-1}, has also been considered. For instance, within the deforested area the values of the change in dW/dt are below the considered uncertainty, with an annual average of 0.07 mm day^{-1}, but increasing significantly outside the deforested area up to 1.07 mm day^{-1}, mainly due to lower ET and C rates.

3.2.3. *Impact of deforestation on the total water budget*

Fig. 12 summarizes the long-term averaged monthly changes in the components of the surface and atmospheric water budget for the Amazon south of 5°S and for areas below 1,000 m a.s.l., between the 2050 deforestation and control experiments. We describe the results for the average of two areas, those inside and outside the total deforested patch. We found that changes in the components vary throughout the year, with the largest changes occurring in the JJA and SON periods for both inside and outside the deforested patch (Fig. 12). For instance, at the surface level, within the deforested patch (Fig. 12a) ET shows the largest decreases during the SON and JJA periods, with JJA being the period of smallest increases in P, which translates into no perceptible changes in surface R but a significant increase in dS/dt. Furthermore, when changes are observed in areas outside the deforested patch (Fig. 12b), at the surface level, changes in ET are almost imperceptible, so that small increases in P during SON and DJF dominate the increase in dS/dt. In other words, in deforested areas, changes in the surface budget (looking at dS/dt) are more controlled by ET (e.g. Pearson's correlation

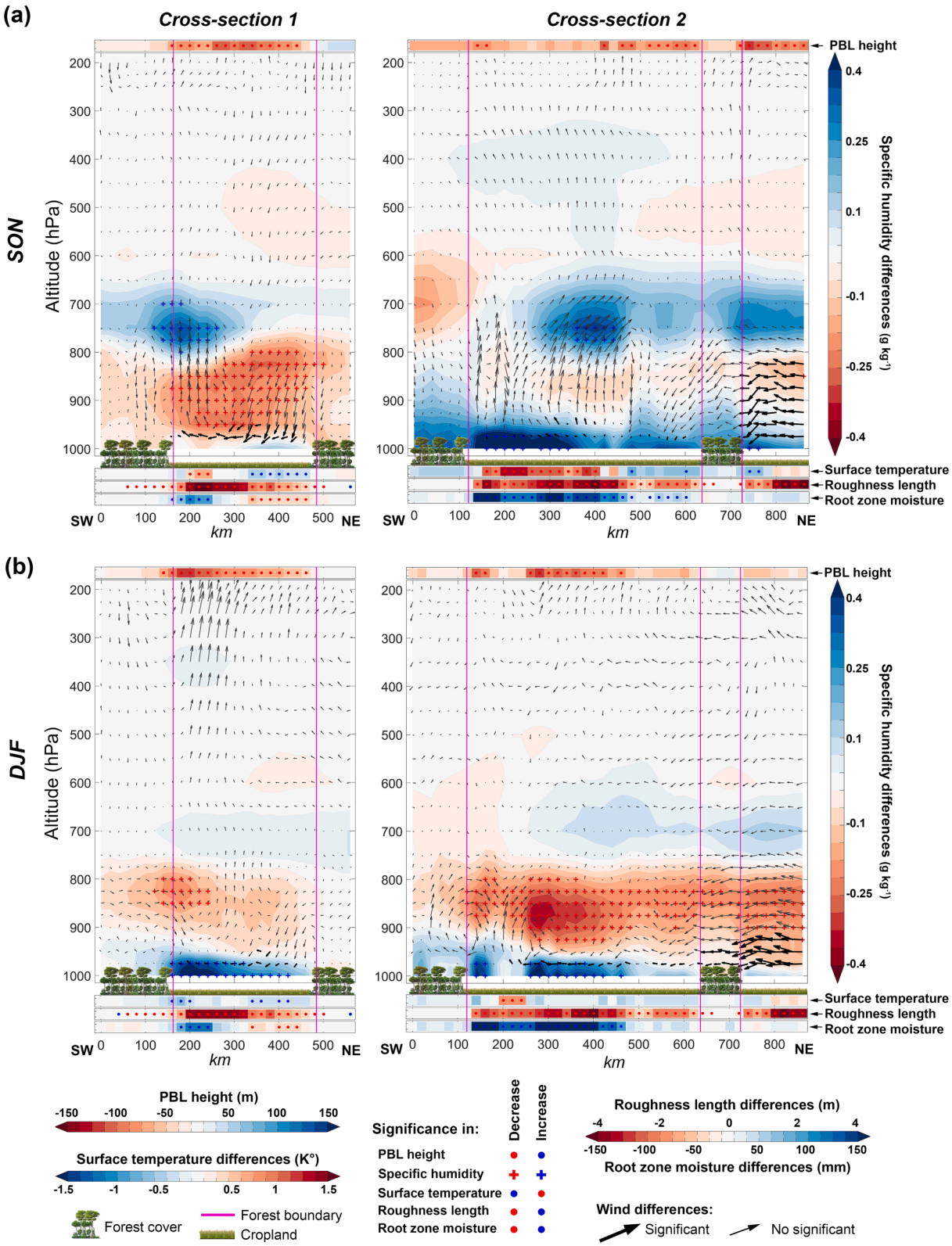

Fig. 10. Differences in atmospheric specific humidity between the 2050 deforestation and control experiments, for (a) SON and (b) DJF seasons for two cross-sections in a southwest (SW) to northeast (NE) direction. Grid points with significant differences show a red or blue cross for decrease or increase, respectively. Changes in the wind velocities are overlaid in regular and bold black arrows for no significant and significant differences, respectively. The bar at the top is from the atmospheric component Planetary boundary layer (PBL) height differences. The three bars at the bottom of each cross-section correspond to the Surface temperature, Roughness length and Root zone moisture differences. Vertical magenta lines delimit the border between forest and cropland. (For interpretation of the references to color in this figure legend, the reader is referred to the web version of this article.)

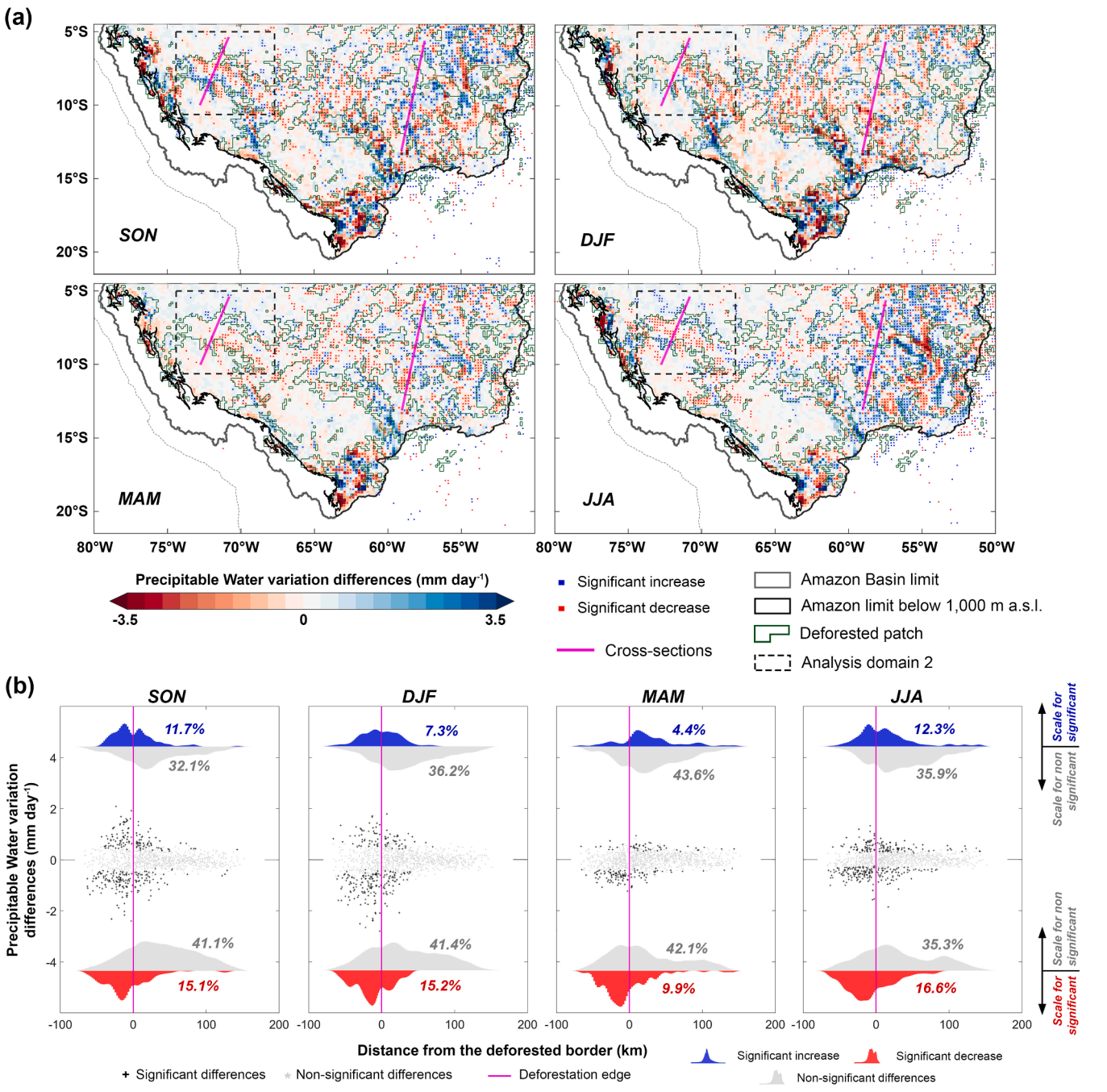

Fig. 11. (a) Maps of precipitable water variation differences between the deforested and control experiments in red to blue color scale. The dashed rectangle represents domain 2 and magenta lines are the cross-sections 1 and 2. Grid points with significant differences show a red or blue dot for decrease or increase, respectively. (b) Differences in precipitable water variation between the 2050 deforestation and control experiments, by season and its relation to the distance to the edge of the deforested patch. For the analysis domain 2 (dotted rectangle), the grid points with significant differences are presented as crosses in black color and their probability of precipitable water variation increase and decrease distribution is shown in blue and red color in a violin plot, respectively, while non-significant variations are shown in gray color. The percentages indicate the proportion of grid points in relation to the total. (For interpretation of the references to color in this figure legend, the reader is referred to the web version of this article.)

coefficient for monthly climatological values between variables, r = -0.62) than by P (r = 0.3), while in non-deforested areas P (r = 0.97) plays a more important role than other components.

At the atmospheric level, P and C vary similarly most of the year except in the dry period (JJA), when C increases more significantly both inside and outside the deforested patch. However, within the deforested patch, ET and C are the components controlling the variation of moisture storage in the atmosphere (dW/dt) with values of Pearson's correlation coefficient r = -0.7 and 0.8, respectively (while P, r = -0.2). However, outside the deforested patch, there is no apparent dominance of a particular component in the budget.

Finally, Fig. 13 shows the annual differences (mm year^{-1}) in the components in a schematic representation averaged for both inside and outside the deforested patch. It was evidenced, on the one hand, that in the RegIPSL model universe, in a 2050 deforestation experiment, the water allocated at the surface (represented by the terrestrial water storage variation (dS/dt)) remains locally wetter (within the deforested patch) compared to the non-deforested one, +68.7 vs + 5.5 mm year^{-1}

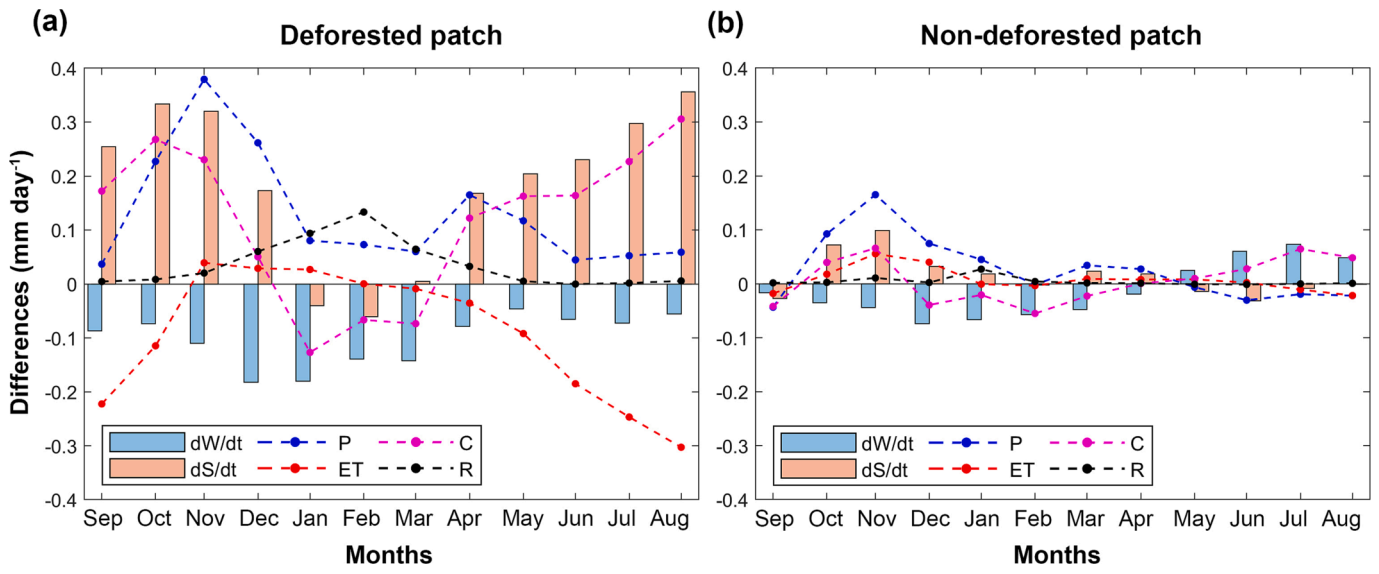

Fig. 12. Long term monthly differences in the main components of the surface and atmospheric water budget, between the 2050 deforestation and control experiments, for the average of the grid points (a) inside and (b) outside of the deforested patch for south of 5°S in the Amazon and for areas below 1,000 m a.s.l.

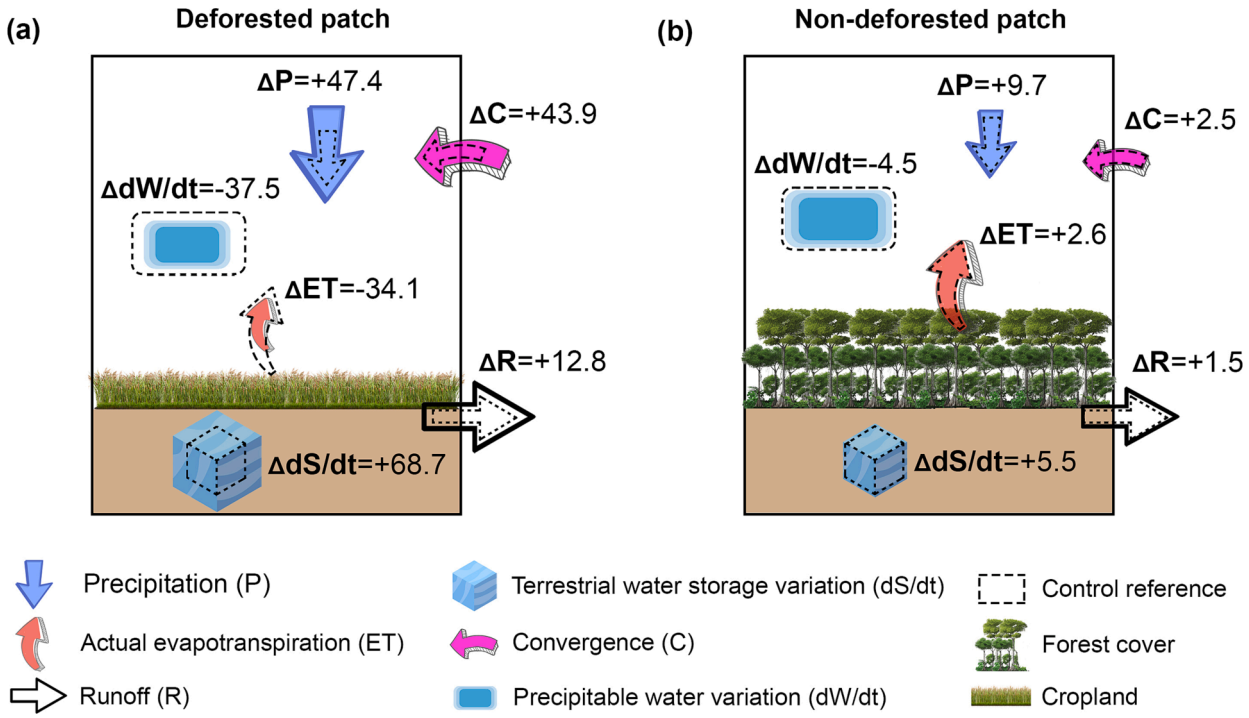

Fig. 13. Schematic representation of the annual differences (mm year^{-1}) in the components of the surface and atmospheric water budget, between the 2050 deforestation and control experiments, for the average of the grid points (a) inside and (b) outside of the deforested patch for south of 5°S in the Amazon and for areas below 1,000 m a.s.l. Black dotted polygons for each component represent schematically RegIPSL control reference values.

(Fig. 13), mainly due to decreases in ET and increases in P. On the other hand, at the atmospheric level, the variation of water storage (represented by the precipitable water variation (dW/dt)) decreases, i.e. the atmosphere is drier within the deforested patch (-37.5 vs −4.5 mm year^{-1}). This last behavior was also found by analyzing the observations (see Fig. S11).

4. Summary and conclusions

The objective of this research was to evaluate the changes in the components of the surface and atmospheric water budget due exclusively to the impacts of land use change, using numerical experiments considering the current and deforested Amazon, the latter based on a scenario for the year 2050. For this purpose, two experiments with the ORCHIDEE surface model coupled to the WRF atmospheric model, denoted here as RegIPSL have been performed for 19 years (2001–2019). Results based on changes between these experiments were evaluated on a seasonal time scale and spatially distributed (~20 km) over the southern region of the Amazon basin.

First, an exhaustive validation of the RegIPSL control experiment was carried out throughout the Amazon basin for most of the model variables used in this research with respect to data based on

observations, remote sensing and models. Based on the performance of statistical indices (e.g. BIAS, KGE and NSE), the RegIPSL control model shows satisfactory results at the monthly level and mainly in the region south of 5°S, which will be the domain of study in this research. These results provide a reliable statistical support considering conditions close to reality for the analysis of the changes in the surface and atmospheric water budget components in relation to a deforestation scenario. It has been shown that significant changes in the main interacting components of the surface and atmospheric water budget (actual evapotranspiration (ET) and precipitation (P)) are sensitive to deforestation rates above 40%. In the case of ET, there is evidence of a decrease associated with a high rate of deforestation, especially in June-November, while for P there is an increase in the September-February period.

Since ET is a key component that connects the land to the atmosphere, linking water, energy and carbon cycles, its changes are closely associated with the extent of deforestation. This translates into evidence that, within the deforested patch, changes in ET dominate changes in surface budget components such as runoff (R) and terrestrial water storage variation (dS/dt), with relatively high correlation values. While atmospheric component such as convergence (C) and precipitable water variation (dW/dt) depend more on the location of the deforested patch than on its deforestation rate.

By analyzing the vertical moisture fluxes in two cross-sections to explain the atmospheric dynamics and spatial behavior of P, C and dW/dt, the hypotheses of previous studies have been evidenced and extended. A dipole occurs during certain seasons (e.g., SON) associated with wind orientation and different sizes of the deforestation pathways. This dipole is evidenced by a suppression of convection (decrease) in the upwind sector, while convection increases in the downwind sector of the deforestation pathway. For medium-sized deforestation pathways (e.g., ~350 km), atmospheric changes are mainly explained by a dynamic effect produced by the decrease in surface roughness. Whereas in large-sized pathways (e.g. ~500 km in the southeastern Amazon) the processes are more complex in which, in addition to the dynamic effect, the thermal effect (increase in surface temperature) is at work.

These cross-sectional analyses show that the triggers for convective processes are associated with many factors such as the scale of the deforestation pathway, which is larger in this study (~500 km in cross-section 2), by seasons as well as by the region analyzed. This highlights the importance of a spatially and temporally distributed analysis of water budget components, as it has been shown that changes can be generated both locally (i.e., ET, P, R and dS/dt) and regionally (i.e., C and dW/dt), varying between seasons.

In general, it has been shown from the RegIPSL model experiments between control and 2050 deforestation that two main characteristic patterns occur: i) there is an increase in the variation of dS/dt in the deforested region, by more than 10 times than in the non-deforested regions. This also occurs at the surface level, where R increases more than 8 times in the deforested area; and ii) a decrease in the variation of atmospheric humidity (for dW/dt) about 8 times drier over the deforested areas compared to the rest of the region; a pattern also detected by observations.

Unlike uncoupled models or studies based solely on observations, the coupled RegIPSL model allows to study deforestation-related processes in a physically coherent system. However, it is important to note that these evidences are framed only in the universe of the RegIPSL model, which can generate a bias due to the representation of model-specific processes. Therefore, future studies should assume the analysis of multiple coupled models to reduce uncertainty in the results. Other studies could also address the use of multiple future projections of climate and deforestation scenarios at the same time.

This study shows that there are complex responses of surface and atmospheric water budget components to deforestation. In that sense, our results can offer a spatialized perspective of the significant changes that could occur in the hydroclimatology of the Amazon if the assumed trend of deforestation continues. Although, in 2012, record low deforestation rates were reached in the Amazonian countries as a result of multiple government initiatives and international pressure, recent records show a trend of increasing deforestation rates since 2013 (Instituto Nacional de Pesquisas Espaciais (INPE), 2020; Nepstad et al., 2014). These values reached the highest levels of the last decade in the Brazilian Amazon in 2020, which has been catalyzed by a series of environmental setbacks. These issues were mainly due to political decisions such as the controversial change in the Brazilian Forestry Code in 2012 (Brancalion et al., 2016), and continued with the weakening of the Brazilian Ministry of Environment's deforestation reduction measures and the disregard of policies related to climate change (Associação Nacional dos Servidores de Meio Ambiente (ASCEMA), 2020; Barlow et al., 2020). This is why this research should draw the attention of decision-makers to propose appropriate resource management policies in the context of land-use planning in all the countries comprising the Amazon region.

Declaration of Competing Interest

The authors declare that they have no known competing financial interests or personal relationships that could have appeared to influence the work reported in this paper.

Data availability

Data will be made available on request.

Acknowledgments

This research has been supported by the French AMANECER-MOPGA project funded by ANR and IRD (ref. ANR-18-MPGA-0008), by the ACE-Amazon project funded by the regional program CLIMAT-AmSud (21-CLIMAT-01), and by the MINCYT-ECOS Sud: A18D04 and INSU LEFE ref 12962. At the same time, this work was granted access to the HPC resources of IDRIS under the allocation 2021-101054 made by GENCI. Simulations were run on the Jean Zay super computer at the French computing center IDRIS. The authors would also like to thank the following agencies/organizations for providing access to data: The Climate Hazards Group Infrared Precipitation for providing CHIRPS, GloH2O group for providing MSWEP, GSFC/DAAC and NASA for providing the TMPA and GPM_IMERGM, Ghent University for providing GLEAM, the eartH2Observe project for WRR-2 outputs from global models (HTESSEL-CaMa, JULES, LISFLOOD, ORCHIDEE, PCR-GLOBWR, SURFEX-TRIP, W3 and WaterGAP3), Paca, V. H. d. M. (2019) for providing ET-Amazon, the European Space Agency (ESA) Climate Change Initiative (CCI) and the Copernicus Climate Change Service (C3S) for providing the Global Land Cover maps and ERA5, the Jet Propulsion Laboratory (JPL), the University of Texas Center for Space Research (CSR) and the Geo Forschungs Zentrum (GFZ) Potsdam for providing GRACE.

Appendix A. Supplementary data

Supplementary data to this article can be found online at https://doi.org/10.1016/j.jhydrol.2023.130082.

References

Abe, C.A., Lobo, F.L., Novo, E.M.L. de M., Costa, M., Dibike, Y., 2019. Modeling the effects of land cover change on sediment concentrations in a gold-mined Amazonian basin. Reg. Environ. Chang. 19, 1801–1813. https://doi.org/10.1007/s10113-019-01513-8.

Alves de Oliveira, B.F., Bottino, M.J., Nobre, P., Nobre, C.A., 2021. Deforestation and climate change are projected to increase heat stress risk in the Brazilian Amazon. Commun Earth Environ 2, 207. https://doi.org/10.1038/s43247-021-00275-8.

Avissar, R., Schmidt, T., 1998. An Evaluation of the Scale at which Ground-Surface Heat Flux Patchiness Affects the Convective Boundary Layer Using Large-Eddy

Simulations. J. Atmos. Sci. 55, 2666–2689. https://doi.org/10.1175/1520-0469(1998)055<2666:AEOTSA>2.0.CO;2.
Avissar, R., Werth, D., 2005. Global Hydroclimatological Teleconnections Resulting from Tropical Deforestation. J. Hydrometeorol. 6, 134–145. https://doi.org/10.1175/JHM406.1.
Balsamo, G., Boussetta, S., Dutra, E., Beljaars, A., Viterbo, P., van den Hurk, B., 2011. Evolution of land-surface processes in the IFS. 10.21957/X1J3I7BZ.
Barella-Ortiz, A., Polcher, J., Tuzet, A., Laval, K., 2013. Potential evaporation estimation through an unstressed surface-energy balance and its sensitivity to climate change. Hydrol. Earth Syst. Sci. 17, 4625–4639. https://doi.org/10.5194/hess-17-4625-2013.
Barlow, J., Berenguer, E., Carmenta, R., França, F., 2020. Clarifying Amazonia's burning crisis. Glob. Chang. Biol. 26, 319–321. https://doi.org/10.1111/gcb.14872.
Beck, H.E., van Dijk, A.I.J.M., Levizzani, V., Schellekens, J., Miralles, D.G., Martens, B., de Roo, A., 2016. MSWEP: 3-hourly 0.25° global gridded precipitation (1979–2015) by merging gauge, satellite, and reanalysis data. Hydrology and Earth System Sciences Discussions 1–38. 10.5194/hess-2016-236.
Beck, H.E., Vergopolan, N., Pan, M., Levizzani, V., van Dijk, A.I.J.M., Weedon, G.P., Brocca, L., Pappenberger, F., Huffman, G.J., Wood, E.F., 2017. Global-scale evaluation of 22 precipitation datasets using gauge observations and hydrological modeling. Hydrol. Earth Syst. Sci. 21, 6201–6217. https://doi.org/10.5194/hess-21-6201-2017.
Best, M.J., Pryor, M., Clark, D.B., Rooney, G.G., Essery, R.L.H., Ménard, C.B., Edwards, J. M., Hendry, M.A., Porson, A., Gedney, N., Mercado, L.M., Sitch, S., Blyth, E., Boucher, O., Cox, P.M., Grimmond, C.S.B., Harding, R.J., 2011. The Joint UK Land Environment Simulator (JULES), model description – Part 1: Energy and water fluxes. Geosci. Model Dev. 4, 677–699. https://doi.org/10.5194/gmd-4-677-2011.
Bontemps, S., Defourny, P., Radoux, J., Van Bogaert, E., Lamarche, C., Achard, F., Mayaux, P., Boettcher, M., Brockmann, C., Kirches, G., Zulkhe, M., Kalogirou, V., Seifert, F.M., Arino, O., 2013. Consistent Global Land Cover Maps For Climate Modelling Communities: Current Achievements Of The ESA' Land Cover CCI 722, 62.
Brancalion, P.H.S., Garcia, L.C., Loyola, R., Rodrigues, R.R., Pillar, V.D., Lewinsohn, T. M., 2016. Análise crítica da Lei de Proteção da Vegetação Nativa (2012), que substituiu o antigo Código Florestal: atualizações e ações em curso. Natureza & Conservação 14, e1–e16. https://doi.org/10.1016/j.ncon.2016.03.004.
Brando, P.M., Balch, J.K., Nepstad, D.C., Morton, D.C., Putz, F.E., Coe, M.T., Silvério, D., Macedo, M.N., Davidson, E.A., Nóbrega, C.C., Alencar, A., Soares-Filho, B.S., 2014. Abrupt increases in Amazonian tree mortality due to drought-fire interactions. PNAS 111, 6347–6352. https://doi.org/10.1073/pnas.1305499111.
Brandon, K., 2014. Ecosystem Services from Tropical Forests: Review of Current Science (SSRN Scholarly Paper No. 2622749). Social Science Research Network, Rochester, NY. 10.2139/ssrn.2622749.
Builes-Jaramillo, A., Poveda, G., 2018. Conjoint Analysis of Surface and Atmospheric Water Balances in the Andes-Amazon System. Water Resour. Res. 54, 3472–3489. https://doi.org/10.1029/2017WR021338.
Carmona Duque, A.M., 2015. Impacts of climate change and climate variability on the spatio-temporal hydrological dynamics of Amazonia.
Casagrande, E., Recanati, F., Rulli, M.C., Bevacqua, D., Melià, P., 2021. Water balance partitioning for ecosystem service assessment. A case study in the Amazon. Ecol. Ind. 121, 107155 https://doi.org/10.1016/j.ecolind.2020.107155.
Clark, D.B., Mercado, L.M., Sitch, S., Jones, C.D., Gedney, N., Best, M.J., Pryor, M., Rooney, G.G., Essery, R.L.H., Blyth, E., Boucher, O., Harding, R.J., Huntingford, C., Cox, P.M., 2011. The Joint UK Land Environment Simulator (JULES), model description – Part 2: Carbon fluxes and vegetation dynamics. Geosci. Model Dev. 4, 701–722. https://doi.org/10.5194/gmd-4-701-2011.
Costa, M.H., Borma, L.S., Espinoza, J.-C., Marcia, M., Marengo, J.A., Marra, D.M., Ometto, J.P., Gatti, L.V., 2021. Chapter 5: The Physical hydroclimate system of the Amazon, in: Nobre, C., Encalada, A., Anderson, E., Roca Alcazar, F.H., Bustamante, M., Mena, C., Peña-Claros, M., Poveda, G., Rodriguez, J.P., Saleska, S., Trumbore, S. E., Val, A., Villa Nova, L., Abramovay, R., Alencar, A., Rodriguez Alzza, A.C., Armenteras, D., Artaxo, P., Athayde, S., Barretto Filho, H.T., Barlow, J., Berenguer, E., Bortolotto, F., Costa, F. de A., Costa, M.H., Cuvi, N., Fearnside, P., Ferreira, J., Flores, B.M., Frieri, S., Gatti, L.V., Guayasamin, J.M., Hecht, S., Hirota, M., Hoorn, C., Josse, C., Lapola, D.M., Larrea, C., Larrea-Alcazar, D.M., Lehm Ardaya, Z., Malhi, Y., Marengo, J.A., Melack, J., Moraes R., M., Moutinho, P., Murmis, M.R., Neves, E. G., Paez, B., Painter, L., Ramos, A., Rosero-Peña, M.C., Schmink, M., Sist, P., ter Steege, H., Val, P., van der Voort, H., Varese, M., Zapata-Ríos, G. (Eds.), Amazon Assessment Report 2021. UN Sustainable Development Solutions Network (SDSN). 10.55161/HTSD9250.
Davidson, E.A., De Araüjo, A.C., Artaxo, P., Balch, J.K., Brown, I.F., Mercedes, M.M., Coe, M.T., Defries, R.S., Keller, M., Longo, M., Munger, J.W., Schroeder, W., Soares-Filho, B.S., Souza, C.M., Wofsy, S.C., 2012. The Amazon basin in transition. Nature 481, 321–328. https://doi.org/10.1038/nature10717.
Davidson, N.C., Fluet-Chouinard, E., Finlayson, C.M., 2018. Global extent and distribution of wetlands: Trends and issues. Mar. Freshw. Res. 69, 620–627. https://doi.org/10.1071/MF17019.
Davison, J.H., Hwang, H.-T., Sudicky, E.A., Mallia, D.V., Lin, J.C., 2018. Full Coupling Between the Atmosphere, Surface, and Subsurface for Integrated Hydrologic Simulation. J. Adv. Model. Earth Syst. 10, 43–53. https://doi.org/10.1002/2017MS001052.
de Rosnay, P., Polcher, J., 1998. Modelling root water uptake in a complex land surface scheme coupled to a GCM. Hydrol. Earth Syst. Sci. 2, 239–255. https://doi.org/10.5194/hess-2-239-1998.
Debortoli, N.S., Dubreuil, V., Funatsu, B., Delahaye, F., de Oliveira, C.H., Rodrigues-Filho, S., Saito, C.H., Fetter, R., 2015. Rainfall patterns in the Southern Amazon: a chronological perspective (1971–2010). Clim. Change 132, 251–264. https://doi.org/10.1007/s10584-015-1415-1.
Debortoli, N.S., Dubreuil, V., Hirota, M., Filho, S.R., Lindoso, D.P., Nabucet, J., 2017. Detecting deforestation impacts in Southern Amazonia rainfall using rain gauges. Int. J. Climatol. 37, 2889–2900. https://doi.org/10.1002/joc.4886.
Decharme, B., Boone, A., Delire, C., Noilhan, J., 2011. Local evaluation of the Interaction between Soil Biosphere Atmosphere soil multilayer diffusion scheme using four pedotransfer functions. J. Geophys. Res. Atmos. 116 https://doi.org/10.1029/2011JD016002.
Decharme, B., Martin, E., Faroux, S., 2013. Reconciling soil thermal and hydrological lower boundary conditions in land surface models. J. Geophys. Res. Atmos. 118, 7819–7834. https://doi.org/10.1002/jgrd.50631.
Diaz, S., Tilman, D., Fargione, J., 2005. Biodiversity regulation of ecosystem services. Ecosystems and Human Well-being: Current State and Trends 297–329.
Dominguez, F., Eiras-Barca, J., Yang, Z., Bock, D., Nieto, R., Gimeno, L., 2022. Amazonian moisture recycling revisited using WRF with water vapor tracers. J. Geophys. Res. Atmos. 127.
Dos Santos, V., Laurent, F., Abe, C., Messner, F., 2018. Hydrologic Response to Land Use Change in a Large Basin in Eastern Amazon. Water 10, 429. https://doi.org/10.3390/w10040429.
Dutra, E., Gianpaolo, Balsamo, Jean-Christophe Calvet, Munier, S., Burke, S., Fink, G., Dijk, A.V., Torre, A.M.-D.L., Beek, R.V., Roo, A.D., Polcher, J., 2017. Report on the improved Water Resources Reanalysis. 10.13140/RG.2.2.14523.67369.
Eiras-Barca, J., Dominguez, F., Yang, Z., Chug, D., Nieto, R., Gimeno, L., Miguez-Macho, G., 2020. Changes in South American hydroclimate under projected Amazonian deforestation. Ann. N.Y. Acad. Sci. 1472, 104–122. https://doi.org/10.1111/nyas.14364.
Espinoza, J.-C., Arias, P.A., Moron, V., Junquas, C., Segura, H., Sierra-Pérez, J.P., Wongchuig, S., Condom, T., 2021. Recent changes in the atmospheric circulation patterns during the dry-to-wet transition season in south tropical South America (1979–2020): Impacts on precipitation and fire season. J. Clim. 34, 9025–9042.
Espinoza, J.C., Chavez, S., Ronchail, J., Junquas, C., Takahashi, K., Lavado, W., 2015. Rainfall hotspots over the south tropical andes: spatial distribution, rainfall intensity and relations with largescale atmospheric circulation. Water Resour. Res. 51, 3459–3475. https://doi.org/10.1002/2014wr016273.
Fassoni-Andrade, A.C., Fleischmann, A.S., Papa, F., de Paiva, R.C.D., Wongchuig, S., Melack, J.M., Moreira, A.A., Paris, A., Ruhoff, A., Barbosa, C., Faria, C., Maciel, D.A., Novo, E.M.L. de M., Durand, F., Frappart, F., Aires, F., Abrahão, G.M., Ferreira-Ferreira, J., Espinoza, J.C., Laipelt, L., Costa, M.H., Espinoza-Villar, R., Calmant, S., Pellet, V., 2021. Amazon hydrology from space: scientific advances and future challenges. Rev. Geophys. https://doi.org/10.1029/2020RG000728.
Feddema, J.J., Oleson, K.W., Bonan, G.B., Mearns, L.O., Buja, L.E., Meehl, G.A., Washington, W.M., 2005. The Importance of Land-Cover Change in Simulating Future Climates. Science 310, 1674–1678. https://doi.org/10.1126/science.1118160.
Feng, S., Fu, Q., 2013. Expansion of global drylands under a warming climate. Atmos. Chem. Phys. 13, 10081–10094. https://doi.org/10.5194/acp-13-10081-2013.
Flörke, M., Kynast, E., Bärlund, I., Eisner, S., Wimmer, F., Alcamo, J., 2013. Domestic and industrial water uses of the past 60 years as a mirror of socio-economic development: A global simulation study. Glob. Environ. Chang. 23, 144–156. https://doi.org/10.1016/j.gloenvcha.2012.10.018.
Fu, R., Yin, L., Li, W., Arias, P.A., Dickinson, R.E., Huang, L., Chakraborty, S., Fernandes, K., Liebmann, B., Fisher, R., Myneni, R.B., 2013. Increased dry-season length over southern Amazonia in recent decades and its implication for future climate projection. PNAS 110, 18110–18115. https://doi.org/10.1073/pnas.1302584110.
Funk, C., Peterson, P., Landsfeld, M., Pedreros, D., Verdin, J., Shukla, S., Husak, G., Rowland, J., Harrison, L., Hoell, A., Michaelsen, J., 2015. The climate hazards infrared precipitation with stations - A new environmental record for monitoring extremes. Sci. Data 2, 1–21. https://doi.org/10.1038/sdata.2015.66.
Getirana, A.C.V., Dutra, E., Guimberteau, M., Kam, J., Li, H.-Y., Decharme, B., Zhang, Z., Ducharne, A., Boone, A., Balsamo, G., Rodell, M., Toure, A.M., Xue, Y., Peters-Lidard, C.D., Kumar, S.V., Arsenault, K., Drapeau, G., Ruby Leung, L., Ronchail, J., Sheffield, J., 2014. Water Balance in the Amazon Basin from a Land Surface Model Ensemble. J. Hydrometeorol. 15, 2586–2614. https://doi.org/10.1175/JHM-D-14-0068.1.
Gomes, V.H.F., Vieira, I.C.G., Salomão, R.P., ter Steege, H., 2019. Amazonian tree species threatened by deforestation and climate change. Nat. Clim. Chang. 9, 547–553. https://doi.org/10.1038/s41558-019-0500-2.
Grell, G.A., Freitas, S.R., 2013. A scale and aerosol aware stochastic convective parameterization for weather and air quality modeling (preprint). Clouds and Precipitation/Atmospheric Modelling/Troposphere/Physics (physical properties and processes). 10.5194/acpd-13-23845-2013.
Guimberteau, M., Drapeau, G., Ronchail, J., Sultan, B., Polcher, J., Martinez, J.-M., Prigent, C., Guyot, J.-L., Cochonneau, G., Espinoza, J.C., Filizola, N., Fraizy, P., Lavado, W., De Oliveira, E., Pombosa, R., Noriega, L., Vauchel, P., 2012. Discharge simulation in the sub-basins of the Amazon using ORCHIDEE forced by new datasets. Hydrol. Earth Syst. Sci. 16, 911–935. https://doi.org/10.5194/hess-16-911-2012.
Guimberteau, M., Ciais, P., Ducharne, A., Boisier, J.P., Dutra Aguiar, A.P., Biemans, H., De Deurwaerder, H., Galbraith, D., Kruijt, B., Langerwisch, F., Poveda, G., Rammig, A., Rodriguez, D.A., Tejada, G., Thonicke, K., Von Randow, C., Von Randow, R.C.S., Zhang, K., Verbeeck, H., 2017. Impacts of future deforestation and climate change on the hydrology of the Amazon Basin: a multi-model analysis with a new set of land-cover change scenarios. Hydrol. Earth Syst. Sci. 21, 1455–1475. https://doi.org/10.5194/hess-21-1455-2017.

Guimberteau, M., Zhu, D., Maignan, F., Huang, Y., Yue, C., Dantec-Nédélec, S., Ottlé, C., Jornet-Puig, A., Bastos, A., Laurent, P., Goll, D., Bowring, S., Chang, J., Guenet, B., Tifafi, M., Peng, S., Krinner, G., Ducharne, A., Wang, F., Wang, T., Wang, X., Wang, Y., Yin, Z., Lauerwald, R., Joetzjer, E., Qiu, C., Kim, H., Ciais, P., 2018. ORCHIDEE-MICT (v8.4.1), a land surface model for the high latitudes: model description and validation. Geosci. Model Dev. 11, 121–163. https://doi.org/10.5194/gmd-11-121-2018.

Gupta, H.V., Sorooshian, S., Yapo, P.O., 1999. Status of Automatic Calibration for Hydrologic Models: Comparison with Multilevel Expert Calibration. J. Hydrol. Eng. 4, 135–143. https://doi.org/10.1061/(ASCE)1084-0699(1999)4:2(135).

Gupta, H.V., Kling, H., Yilmaz, K.K., Martinez, G.F., 2009. Decomposition of the mean squared error and NSE performance criteria: Implications for improving hydrological modelling. J. Hydrol. 377, 80–91. https://doi.org/10.1016/j.jhydrol.2009.08.003.

Haghtalab, N., Moore, N., Heerspink, B.P., Hyndman, D.W., 2020. Evaluating spatial patterns in precipitation trends across the Amazon basin driven by land cover and global scale forcings. Theor. Appl. Climatol. https://doi.org/10.1007/s00704-019-03085-3.

Hersbach, H., Bell, B., Berrisford, P., Hirahara, S., Horányi, A., Muñoz-Sabater, J., Nicolas, J., Peubey, C., Radu, R., Schepers, D., Simmons, A., Soci, C., Abdalla, S., Abellan, X., Balsamo, G., Bechtold, P., Biavati, G., Bidlot, J., Bonavita, M., De Chiara, G., Dahlgren, P., Dee, D., Diamantakis, M., Dragani, R., Flemming, J., Forbes, R., Fuentes, M., Geer, A., Haimberger, L., Healy, S., Hogan, R.J., Hólm, E., Janisková, M., Keeley, S., Laloyaux, P., Lopez, P., Lupu, C., Radnoti, G., de Rosnay, P., Rozum, I., Vamborg, F., Villaume, S., Thépaut, J.N., 2020. The ERA5 global reanalysis. Q. J. R. Meteorolog. Soc. 1–51 https://doi.org/10.1002/qj.3803.

Hubbell, S.P., He, F., Condit, R., Borda-de-Água, L., Kellner, J., ter Steege, H., 2008. How many tree species are there in the Amazon and how many of them will go extinct? Proc. Natl. Acad. Sci. 105, 11498–11504. https://doi.org/10.1073/pnas.0801915105.

Huffman, G.J., Bolvin, D.T., Nelkin, E.J., Wolff, D.B., Adler, R.F., Gu, G., 2007. The TRMM Multisatellite Precipitation Analysis (TMPA): quasi-global, multiyear, combined-sensor precipitation estimates at fine scales. J. Hydrometeorol. 8, 38–55.

Huffman, G.J., Bolvin, D.T., Braithwaite, D., Hsu, K., Joyce, R., Kidd, C., Nelkin, E.J., Sorooshian, S., Tan, J., Xie, P., 2019. NASA Global Precipitation Measurement (GPM) Integrated Multi-Satellite Retrievals for GPM (IMERG) 38.

Iacono, M.J., Delamere, J.S., Mlawer, E.J., Shephard, M.W., Clough, S.A., Collins, W.D., 2008. Radiative forcing by long-lived greenhouse gases: Calculations with the AER radiative transfer models. J. Geophys. Res. 113, D13103. https://doi.org/10.1029/2008JD009944.

Instituto Nacional de Pesquisas Espaciais (INPE), 2020. Portal Terrabrasilis. URL http://terrabrasilis.dpi.inpe.br/en/home-page/ (accessed 5.21.23).

Junquas, C., Heredia, M.B., Condom, T., Ruiz-Hernández, J.C., Campozano, L., Dudhia, J., Espinoza, J.C., Menegoz, M., Rabatel, A., Sicart, J.-E., 2022. Regional climate modeling of the diurnal cycle of precipitation and associated atmospheric circulation patterns over an Andean glacier region (Antisana, Ecuador). Clim. Dyn. 58, 3075–3104.

Kendall, M.G., 1975. Rank Correlation Methods, 4th, Editio. ed. Charles Griffin, London, UK.

Khanna, J., Medvigy, D., 2014. Strong control of surface roughness variations on the simulated dry season regional atmospheric response to contemporary deforestation in Rondônia, Brazil. J. Geophys. Res. Atmos. 119, 13067–13078. https://doi.org/10.1002/2014JD022278.

Khanna, J., Medvigy, D., Fueglistaler, S., Walko, R., 2017. Regional dry-season climate changes due to three decades of Amazonian deforestation. Nature Clim Change 7, 200–204. https://doi.org/10.1038/nclimate3226.

Kling, H., Fuchs, M., Paulin, M., 2012. Runoff conditions in the upper Danube basin under an ensemble of climate change scenarios. J. Hydrol. 424–425, 264–277. https://doi.org/10.1016/j.jhydrol.2012.01.011.

Krinner, G., Viovy, N., de Noblet-Ducoudré, N., Ogée, J., Polcher, J., Friedlingstein, P., Ciais, P., Sitch, S., Prentice, I.C., 2005. A dynamic global vegetation model for studies of the coupled atmosphere-biosphere system. Global Biogeochem. Cycles 19, 1–33. https://doi.org/10.1029/2003GB002199.

Lau, W.K.M., Kim, K.-M., Chern, J.-D., Tao, W.K., Leung, L.R., 2020. Structural changes and variability of the ITCZ induced by radiation–cloud–convection–circulation interactions: inferences from the Goddard Multi-scale Modeling Framework (GMMF) experiments. Clim. Dyn. 54, 211–229. https://doi.org/10.1007/s00382-019-05000-y.

Laurance, W.F., Koster, H., Grooten, M., Anderson, A.B., Zuidema, P.A., Zwick, S., Zagt, R.J., Lynam, A.J., Linkie, M., Anten, N.P.R., 2012. Making conservation research more relevant for conservation practitioners. Biol. Conserv. 153, 164–168. https://doi.org/10.1016/j.biocon.2012.05.012.

Lawrence, P.J., Chase, T.N., 2010. Investigating the climate impacts of global land cover change in the community climate system model. Int. J. Climatol. 30, 2066–2087. https://doi.org/10.1002/joc.2061.

Lawrence, D., Vandecar, K., 2015. Effects of tropical deforestation on climate and agriculture. Nat. Clim. Chang. 5, 27–36. https://doi.org/10.1038/nclimate2430.

Le Page, Y., Morton, D., Hartin, C., Bond-Lamberty, B., Pereira, J.M.C., Hurtt, G., Asrar, G., 2017. Synergy between land use and climate change increases future fire risk in Amazon forests. Earth Syst. Dyn. 8, 1237–1246. https://doi.org/10.5194/esd-8-1237-2017.

Leite-Filho, A.T., de Sousa Pontes, V.Y., Costa, M.H., 2019. Effects of Deforestation on the Onset of the Rainy Season and the Duration of Dry Spells in Southern Amazonia. J. Geophys. Res. Atmos. 124, 5268–5281. https://doi.org/10.1029/2018JD029537.

Maeda, E.E., Kim, H., Aragão, L.E.O.C., Famiglietti, J.S., Oki, T., 2015. Disruption of hydroecological equilibrium in southwest Amazon mediated by drought. Geophys. Res. Lett. 42, 7546–7553. https://doi.org/10.1002/2015GL065252.

Malhi, Y., Roberts, J.T., Betts, R.A., Killeen, T.J., Li, W., Nobre, C.A., 2008. Climate change, deforestation, and the fate of the Amazon. Science 319, 169–172. https://doi.org/10.1126/science.1146961.

Malik, K.M., Taylor, P.A., 2011. Characteristics of Moisture Flux Convergence over the Mackenzie River Basin for Water Years 1991–2008. Atmos. Ocean 49, 279–288. https://doi.org/10.1080/07055900.2011.609528.

Marengo, J.A., Soares, W.R., Saulo, C., Nicolini, M., 2004. Climatology of the Low-Level Jet East of the Andes as Derived from the NCEP–NCAR Reanalyses: Characteristics and Temporal Variability. J. Clim. 17, 2261–2280. https://doi.org/10.1175/1520-0442(2004)017<2261:COTLJE>2.0.CO;2.

Medvigy, D., Walko, R.L., Otte, M.J., Avissar, R., 2013. Simulated Changes in Northwest U.S. Climate in Response to Amazon Deforestation*. J. Clim. 26, 9115–9136. https://doi.org/10.1175/JCLI-D-12-00775.1.

Morrison, H., Thompson, G., Tatarskii, V., 2009. Impact of Cloud Microphysics on the Development of Trailing Stratiform Precipitation in a Simulated Squall Line: Comparison of One- and Two-Moment Schemes. Mon. Weather Rev. 137, 991–1007. https://doi.org/10.1175/2008MWR2556.1.

Associação Nacional dos Servidores de Meio Ambiente (ASCEMA), 2020. Cronologia de um Desastre Anunciado: Ações do Governo Bolsonaro para Desmontar as Políticas de Meio Ambiente no Brasil. URL https://go.nature.com/39pfY29.

Nakanishi, M., Niino, H., 2006. An Improved Mellor-Yamada Level-3 Model: Its Numerical Stability and Application to a Regional Prediction of Advection Fog. Boundary-Layer Meteorol 119, 397–407. https://doi.org/10.1007/s10546-005-9030-8.

Nash, J.E., Sutcliffe, J.V., 1970. River flow forecasting through conceptual models part I — A discussion of principles. J. Hydrol. 10, 282–290. https://doi.org/10.1016/0022-1694(70)90255-6.

Nepstad, D., McGrath, D., Stickler, C., Alencar, A., Azevedo, A., Swette, B., Bezerra, T., DiGiano, M., Shimada, J., Seroa da Motta, R., Armijo, E., Castello, L., Brando, P., Hansen, M.C., McGrath-Horn, M., Carvalho, O., Hess, L., 2014. Slowing Amazon deforestation through public policy and interventions in beef and soy supply chains. Science 344, 1118–1123. https://doi.org/10.1126/science.1248525.

Nobre, C.A., Borma, L.D.S., 2009. "Tipping points" for the Amazon forest. Curr. Opin. Environ. Sustain. 1, 28–36. https://doi.org/10.1016/j.cosust.2009.07.003.

Nobre, C.A., Sampaio, G., Borma, L.S., Castilla-Rubio, J.C., Silva, J.S., Cardoso, M., 2016. Land-use and climate change risks in the amazon and the need of a novel sustainable development paradigm. Proceedings of the National Academy of Sciences of the United States of America 113, 10759–10768. 10.1073/pnas.1605516113.

Nobre, P., Malagutti, M., Urbano, D.F., de Almeida, R.A.F., Giarolla, E., 2009. Amazon Deforestation and Climate Change in a Coupled Model Simulation. J. Clim. 22, 5686–5697. https://doi.org/10.1175/2009JCLI2757.1.

Paca, V.H. da M., Espinoza-Dávalos, G.E., Hessels, T.M., Moreira, D.M., Comair, G.F., Bastiaanssen, W.G.M., 2019. The spatial variability of actual evapotranspiration across the Amazon River Basin based on remote sensing products validated with flux towers. Ecol. Process. 8 https://doi.org/10.1186/s13717-019-0158-8.

Patton, E.G., Sullivan, P.P., Moeng, C.-H., 2005. The Influence of Idealized Heterogeneity on Wet and Dry Planetary Boundary Layers Coupled to the Land Surface. J. Atmos. Sci. 62, 2078–2097. https://doi.org/10.1175/JAS3465.1.

Posada-Marín, J.A., Salazar, J.F., 2022. River flow response to deforestation: Contrasting results from different models. Water Security 15, 100115. https://doi.org/10.1016/j.wasec.2022.100115.

Rao, V.B., Chapa, S.R., Cavalcanti, I.F.A., 1998. Moisture budget in the tropics and the Walker circulation. J. Geophys. Res. Atmos. 103, 13713–13728. https://doi.org/10.1029/98JD00943.

Rodriguez, D.A., Tomasella, J., Linhares, C., 2018. Is the forest conversion to pasture affecting the hydrological response of Amazonian catchments? Signals in the Ji-Paraná Basin. Hydrol. Process. 24, 1254–1269. https://doi.org/10.1002/hyp.7586.

Rosales, A.G., Junquas, C., da Rocha, R.P., Condom, T., Espinoza, J.-C., 2022. Valley-Mountain Circulation Associated with the Diurnal Cycle of Precipitation in the Tropical Andes (Santa River Basin, Peru). Atmos. 13, 344.

Salati, E., Nobre, C.A., 1991. Possible climatic impacts of tropical deforestation. Clim. Change 19, 177–196. https://doi.org/10.1007/BF00142225.

Salazar Villegas, J.F., Poveda Jaramillo, G., Salazar Velásquez, L.F., 2006. Balances hidrológicos y estimación de caudales extremos en la Amazonia.

Saleska, S.R., da Rrocha, H.R., Huete, A.R., Nobre, A.D., Artaxo, P., Shimabukuro, Y.E., 2013. LBA-ECO CD-32 Flux Tower Network Data Compilation, Brazilian Amazon: 1999-2006 267.05443 MB. 10.3334/ORNLDAAC/1174.

Schrapffer, A., Sörensson, A., Polcher, J., Fita, L., 2020. Benefits of representing floodplains in a Land Surface Model: Pantanal simulated with ORCHIDEE CMIP6 version. Clim. Dyn. 55, 1303–1323. https://doi.org/10.1007/s00382-020-05324-0.

Sierra, J.P., Junquas, C., Espinoza, J.C., Segura, H., Condom, T., Andrade, M., Molina-Carpio, J., Ticona, L., Mardoñez, V., Blacutt, L., 2022. Deforestation impacts on Amazon-Andes hydroclimatic connectivity. Clim. Dyn. 58, 2609–2636.

Singh, J., Knapp, H.V., Arnold, J.G., Demissie, M., 2005. Hydrological modeling of the Iroquois river watershed using HSPF and SWAT. J Am Water Resources Assoc 41, 343–360. https://doi.org/10.1111/j.1752-1688.2005.tb03740.x.

Skamarock, C., Klemp, B., Dudhia, J., Gill, O., Barker, D., Duda, G., Huang, X., Wang, W., Powers, G., 2008. A Description of the Advanced Research WRF Version 3. 10.5065/D68S4MVH.

Soares-Filho, B.S., Nepstad, D.C., Curran, L.M., Cerqueira, G.C., Garcia, R.A., Ramos, C. A., Voll, E., McDonald, A., Lefebvre, P., Schlesinger, P., 2006. Modelling conservation in the Amazon basin. Nature 440, 520–523. https://doi.org/10.1038/nature04389.

Soares-Filho, B.S., Nepstad, D.C., Curran, L.M., Voll, E., Garcia, R.A., Ramos, C.A., McDonald, A.J., Lefebvre, P.A., Schlesinger, P., 2013. LBA-ECO LC-14 Modeled

Deforestation Scenarios. Amazon Basin 2002–2050. https://doi.org/10.3334/ORNLDAAC/1153.

Song, X.-P., Hansen, M.C., Potapov, P., Adusei, B., Pickering, J., Adami, M., Lima, A., Zalles, V., Stehman, S.V., Di Bella, C.M., Conde, M.C., Copati, E.J., Fernandes, L.B., Hernandez-Serna, A., Jantz, S.M., Pickens, A.H., Turubanova, S., Tyukavina, A., 2021. Massive soybean expansion in South America since 2000 and implications for conservation. Nat Sustain 4, 784–792. https://doi.org/10.1038/s41893-021-00729-z.

Stickler, C.M., Coe, M.T., Costa, M.H., Nepstad, D.C., McGrath, D.G., Dias, L.C.P., Rodrigues, H.O., Soares-Filho, B.S., 2013. Dependence of hydropower energy generation on forests in the Amazon Basin at local and regional scales. Proceedings of the National Academy of Sciences 110, 9601–9606. 10.1073/pnas.1215331110.

Strong, G. s., Proctor, B., Wang, M., Soulis, E. d., Smith, C. d., Seglenieks, F., Snelgrove, K., 2002. Closing the Mackenzie basin water budget, water years 1994/95 to 1996/97. null 40, 113–124. 10.3137/ao.400203.

Sutanudjaja, E.H., van Beek, R., Wanders, N., Wada, Y., Bosmans, J.H.C., Drost, N., van der Ent, R.J., de Graaf, I.E.M., Hoch, J.M., de Jong, K., Karssenberg, D., López López, P., Peßenteiner, S., Schmitz, O., Straatsma, M.W., Vannametee, E., Wisser, D., Bierkens, M.F.P., 2018. PCR-GLOBWB 2: a 5 arcmin global hydrological and water resources model. Geosci. Model Dev. 11, 2429–2453. https://doi.org/10.5194/gmd-11-2429-2018.

Tapley, B.D., Bettadpur, S., Ries, J.C., Thompson, P.F., Watkins, M.M., 2004. GRACE measurements of mass variability in the Earth system. Science 305, 503–505. https://doi.org/10.1126/science.1099192.

van Beek, L.P.H., Wada, Y., Bierkens, M.F.P., 2011. Global monthly water stress: 1. Water balance and water availability. Water Resources Research 47. 10.1029/2010WR009791.

Van Der Knijff, J.M., Younis, J., De Roo, A.P.J., 2010. LISFLOOD: a GIS-based distributed model for river basin scale water balance and flood simulation. Int. J. Geogr. Inf. Sci. 24, 189–212. https://doi.org/10.1080/13658810802549154.

van Dijk, A.I.J.M., Schellekens, J., Yebra, M., Beck, H.E., Renzullo, L.J., Weerts, A., Donchyts, G., 2018. Global 5 km resolution estimates of secondary evaporation including irrigation through satellite data assimilation. Hydrol. Earth Syst. Sci. 22, 4959–4980. https://doi.org/10.5194/hess-22-4959-2018.

van Dijk, A., 2010. AWRA Technical Report 3. Landscape Model (version 0.5) Technical Description.

Verzano, K., 2009. Climate change impacts on flood related hydrological processes: Further development and application of a global scale hydrological model 26644480. 10.17617/2.993926.

von Storch, H., Langenberg, H., Feser, F., 2000. A Spectral Nudging Technique for Dynamical Downscaling Purposes. Mon. Weather Rev. 128, 3664–3673. https://doi.org/10.1175/1520-0493(2000)128<3664:ASNTFD>2.0.CO;2.

Wagner, S., Fersch, B., Yuan, F., Yu, Z., Kunstmann, H., 2016. Fully coupled atmospheric-hydrological modeling at regional and long-term scales: Development, application, and analysis of WRF-HMS. Water Resour. Res. 52, 3187–3211. https://doi.org/10.1002/2015WR018185.

Wang, W., Bruyère, C., Duda, M., Dudhia, J., Gill, D., Kavulich, M., Keene, K., Lin, H.-C., Michalakes, J., Rizvi, S., Zhang, X., Berner, judith, Fossell, K., 2016. ARW Version 3 Modeling System User's Guide. National Center for Atmospheric Research.

Wartenburger, R., Seneviratne, S.I., Hirschi, M., Chang, J., Ciais, P., Deryng, D., Elliott, J., Folberth, C., Gosling, S.N., Gudmundsson, L., Henrot, A.-J., Hickler, T., Ito, A., Khabarov, N., Kim, H., Leng, G., Liu, J., Liu, X., Masaki, Y., Morfopoulos, C., Müller, C., Schmied, H.M., Nishina, K., Orth, R., Pokhrel, Y., Pugh, T.A.M., Satoh, Y., Schaphoff, S., Schmid, E., Sheffield, J., Stacke, T., Steinkamp, J., Tang, Q., Thiery, W., Wada, Y., Wang, X., Weedon, G.P., Yang, H., Zhou, T., 2018. Evapotranspiration simulations in ISIMIP2a—Evaluation of spatio-temporal characteristics with a comprehensive ensemble of independent datasets. Environ. Res. Lett. 13, 075001 https://doi.org/10.1088/1748-9326/aac4bb.

Weng, W., Luedeke, M.K.B., Zemp, D.C., Lakes, T., Kropp, J.P., 2018. Aerial and surface rivers: downwind impacts on water availability from land use changes in Amazonia. Hydrol. Earth Syst. Sci. 22, 911–927. https://doi.org/10.5194/hess-22-911-2018.

Wongchuig, S., Espinoza, J.C., Condom, T., Segura, H., Ronchail, J., Arias, P.A., Junquas, C., Rabatel, A., Lebel, T., 2021. A regional view of the linkages between hydro-climatic changes and deforestation in the Southern Amazon. Int J Climatol joc.7443. 10.1002/joc.7443.

Wongchuig, S., Paiva, R., Espinoza, J.C., Collischonn, W., 2017. Multi-decadal Hydrological Retrospective: Case study of Amazon floods and droughts. J. Hydrol. 549, 667–684. https://doi.org/10.1016/j.jhydrol.2017.04.019.

Wright, J.S., Fu, R., Worden, J.R., Chakraborty, S., Clinton, N.E., Risi, C., Sun, Y., Yin, L., 2017. Rainforest-initiated wet season onset over the southern Amazon. Proceedings of the National Academy of Sciences of the United States of America 114, 8481–8486. 10.1073/pnas.1621516114.

Zemp, D.C., Schleussner, C.F., Barbosa, H.M.J., Hirota, M., Montade, V., Sampaio, G., Staal, A., Wang-Erlandsson, L., Rammig, A., 2017. Self-amplified Amazon forest loss due to vegetation-atmosphere feedbacks. Nat. Commun. 8 https://doi.org/10.1038/ncomms14681.

Zeng, N., Neelin, J.D., 1999. A land-atmosphere interaction theory for the tropical deforestation problem. J. Clim. 12, 857–872. https://doi.org/10.1175/1520-0442(1999)012<0857:alaitf>2.0.co;2.

Zhang, Y., Hou, J., Gu, J., Huang, C., Li, X., 2017. SWAT-Based Hydrological Data Assimilation System (SWAT-HDAS): Description and Case Application to River Basin-Scale Hydrological Predictions. J. Adv. Model. Earth Syst. 9, 2863–2882. https://doi.org/10.1002/2017MS001144.